UNIVERSITY OF CALIFORNIA
RIVERSIDE

Abiotic Oxidation Rate of Chalcopyrite in Seawater: Implications for Seafloor Mining

A Thesis submitted in partial satisfaction
of the requirements for the degree of

Master of Science

in

Geological Sciences

by

Laura Danielle Bilenker

December 2011

Thesis Committee:
Dr. Michael A. McKibben, Chairperson
Dr. Gordon Love
Dr. Timothy Lyons

The Thesis of Laura Danielle Bilenker is approved:

_____

_____

_____
Committee Chairperson

University of California, Riverside

ACKNOWLEDGEMENTS

I would like to thank my advisor, Dr. Michael A. McKibben, for continual guidance and advice (scientific and otherwise) as I pursued my Master's degree, as well as Tim Lyons and Gordon Love for serving on my committee. This project was made possible by funding from the National Science Foundation.

I am also indebted to Jeremy Owens for teaching me the ropes of the ICP-MS, and for his and Steve Bates's infinite patience when things did not go as expected (and even when they did). Also, I could not have asked for better people to spend endless hours with in an office without windows or crowded kinetics lab than Gina Romano and Danielle Montgomery. Last, but certainly not least, I would like to express my gratitude to my amazing family, especially my parents Lanie and Jim. I sincerely appreciate your unwavering support and honest effort to understand what I do and why I do it.

DEDICATION

This Thesis is dedicated to my number one role model in academia, science, and life: my grandfather, Dr. Eugene Bilenker.

ABSTRACT OF THE THESIS

Abiotic Oxidation Rate of Chalcopyrite in Seawater:
Implications for Seafloor Mining

by

Laura Danielle Bilenker

Master of Science, Graduate Program in Geological Sciences
University of California, Riverside, December 2011
Dr. Michael A. McKibben, Chairperson

In situ mining of seafloor massive sulfide (SMS) deposits will have consequences thus far not quantified. On land, interaction of mined sulfide minerals with surface and groundwaters yields acid mine drainage. Pulverization of SMS on the ocean floors will produce highly reactive sulfide mineral surface areas, leading to the localized potential for seafloor acid generation. Chalcopyrite ($CuFeS_2$) is one of several ore minerals found in SMS deposits whose oxidation kinetics need to be quantified to estimate the significance of acid production.

To constrain the oxidation rate of chalcopyrite in seawater, the initial rate experimental method was employed and combined with the isolation method to derive a rate law. Data collected from batch reactor experiments without abundant precipitates (pH <4.5), between 7°C and 25°C, and P_{O_2} from 0.10 to 0.995 atm were incorporated into the rate law. The molal specific rate law is:

$$R_{sp} = - 10^{-9.38}(P_{O2})^{1.22}(H^{+})^{0.36}$$

Chalcopyrite oxidizes slowly in seawater relative to other sulfide minerals like pyrrhotite ($Fe_{1-x}S$), so data from this study establishes a minimum rate of abiotic SMS weathering by oxidation. The slow rate of oxidation of chalcopyrite observed here has positive implications for seafloor mining. Not only will this sulfide not be the main culprit for acid production, but the copper ore will arrive at the surface with minimal dissolution and loss of metal value. Constraining the oxidation rates of individual sulfide mineral species will be useful in modeling SMS mining repercussions, as well as quantifying rates of natural chemical weathering in the oceans over geologic time. This information will be applicable to interpreting the Cu/Fe ratios of VMS deposits.

The potential for local acid generation can be viewed as a microcosm of the global problem of ocean acidification caused by dissolution of anthropogenic atmospheric CO_2. Data show sulfide mineral oxidation rates increase with lower pH, implying that a worldwide drop in ocean pH may amplify the dissolution of SMS deposits, changing the marine ecosystem.

TABLE OF CONTENTS

INTRODUCTION

The oxidation and dissolution of metal sulfide minerals in seawater occurs both naturally, during aging and weathering of seafloor hot spring vents and mounds, and anthropogenically, during seafloor mining. *In situ* mining of seafloor massive sulfide (SMS) deposits will have environmental consequences that are not yet quantified. On land, interaction of mined or exposed sulfide minerals with oxygenated surface and groundwaters can yield acid mine drainage via overall reactions such as:

$$CuFeS_2 + 8.5\ O_{2(aq)} + 5\ H_2O = 8\ H^+ + 4\ SO_4^{2-} + 2\ FeO(OH) + 2\ CuO \qquad \text{(Equation 1)}$$

Likewise, pulverization of SMS on the ocean floors and their exposure to oxygenated seawater during ore extraction, processing and effluent dispersal will produce fresh, highly reactive sulfide mineral surfaces, leading to the localized potential for seafloor acid generation. Chalcopyrite ($CuFeS_2$) is one of several ore minerals found in SMS deposits whose dissolution kinetics in seawater need to be quantified to estimate the significance of acid production.

Chalcopyrite is mined globally for the abundant copper and trace amounts of gold it can contain. For this reason, chalcopyrite is the most important copper ore in the Earth's crust. It is found in various geologic settings, most commonly in hydrothermal deposits (Nesse, 2004).

Within oceanic crust, the heating and convection of seawater through hot basaltic rock above sites of active magmatism result in hydrothermal fluids that are enriched in dissolved sulfur and metals. These fluids rise due to thermal convection, and are vented

from the crust into cold surrounding waters. When they are quenched, dissolved components precipitate as spires and mounds at the ocean-seafloor interface and as particulate plumes above the vents that eventually sink to the seafloor. Abundant Cu-Fe-Pb-Zn sulfide minerals accumulate in the spires and mounds, forming potentially economic SMS deposits (Edmond et al., 1979; Franklin et al., 1981). Seafloor hot springs and SMS deposits form mainly in areas of active extension or volcanism at plate boundaries, such as mid-ocean rift zones or back-arc basins (Edmond et al., 1979; Edmond, et al., 1982; Von Damm et al., 1985; Rona et al., 1986; German et al., 1995; Hannington, 1995). The active sulfide-rich hydrothermal vents are commonly known as "black smokers" and on land, older analogues of SMS deposits are known as volcanogenic massive sulfides (VMS) or volcanic hosted massive sulfides (VHMS) (Robb, 2005).

SMS deposits tend to contain substantially higher ore grades than continental Cu deposits such as porphyry Cu mines, although the tonnage of a typical porphyry mine dwarfs that of a SMS. From a mine like Bingham Canyon in Utah, the Kennecott Utah Copper Corporation extracts ore containing only about 0.7% Cu (Roberts and Sheahan, 1988). In spite of the low ore grade, the total tonnage of Cu at Bingham is enough to provide ~13% of the United States' total copper consumption (Rio Tinto, 2011). With the recent discovery of Cu grades that are at least 10 times higher in SMS deposits, the interest of mining companies has widened to include the seafloor.

In addition to impressive Cu ore grades, another attraction for seafloor SMS mining is the enhanced profitability from co-products such as gold, based on the current metals market. The value of gold has increased persistently from $300/ounce in January 2000 to over $1750/ounce at the beginning of August 2011 (Figure 1) (Kitco, 2011). Copper prices have not skyrocketed as dramatically, but have quadrupled over the past couple of years. The growing demand for both of these metals is conducive to exploring "unconventional mineral resources" like SMS deposits (Shanks, 1983).

Exploratory drilling and surveying efforts by pioneer seafloor mining companies have identified numerous potential SMS mining locations in shallow ocean basins. Because of the political complexities of seabed law in international waters, it is more feasible for mining companies to begin at sites located within the Exclusive Economic Zones (EEZs) of individual coastal nations (Figure 2). This reduces the challenges associated with exploiting deep sea sulfide deposits mainly to technological ones such as extreme conditions (depth, heat, salinity, acidity). Inactive vents and mounds are physically accessible and relatively safe to work on, compared with active vents.

Recent drilling reports on a candidate mining site in the Bismarck Sea catalogue the presence of 10 meter tall high-grade massive sulfide spires and an 18+ meter thick SMS zone below the ocean floor (Nautilus, 2007). About one quarter of this material is chalcopyrite while almost one half is pyrite (FeS_2). Furthermore, according to a 2007 News Release from Nautilus, the remote drilling technique has been successful up to 1800 meters below the surface of the water. At depths averaging 1500 meters, the ~18

meter thick SMS ore zone is overlain by only a single meter of sediment. Minimal overburden simplifies material retrieval and waste management.

The strategy is to grind the minerals via remotely controlled seafloor mining tools and transport the product through a riser pipe to a ship at the surface. On board, water will be removed, the ore separated, and unneeded slurry filtered to a smaller grain size and returned to the water column (Nautilus, 2008).

During every step of this process, there is the potential for anthropogenically-enhanced sulfide mineral oxidation. Oxidation of chalcopyrite is an irreversible reaction which produces sulfuric acid, as well as dissolved Cu and Fe (ignoring for the moment any subsequent metal precipitation reactions):

$$CuFeS_2 + 3.75\ O_2 + 0.5\ H_2O = H^+ + Fe^{2+} + 2\ SO_4^{2-} + Cu^+ \quad \text{(Equation 2)}$$

At land-based mines, this type of reaction has contributed to Acid Mine Drainage, which is detrimental to animals, vegetation, and humans. Sulfide mineral dissolution rate laws applicable to seafloor conditions will be instrumental in predicting the environmental effects of seafloor mining, and will also enhance our understanding of natural geochemical weathering processes affecting SMS deposits.

Laboratory experiments and *in situ* measurements have been used to determine the reaction rates of many sulfide minerals in various scenarios, primarily in the contexts of continental Acid Mine Drainage and terrestrial sulfide ore hydrometallurgy. The result is an extensive library of rate laws based on differing experimental techniques and material preparation procedures, designed to accomplish a myriad of goals (e.g., Rimstidt

and Dove, 1986; McKibben and Barnes, 1986; Dove and Crerar, 1990; Caldeira et al., 2003; Antonijevic et al., 2004; Acero et al., 2007). Some researchers have previously addressed the effect of chlorine ions on the oxidation rates of chalcopyrite and dissolved copper (Lu et al., 2000; González-Dávila et al., 2009; Ruiz et al., 2011), finding that the presence of higher Cl^- concentrations accelerate the rate. So far, though, no experimental kinetic work on chalcopyrite has been completed in natural or synthetic seawater (Kimball et al., 2010).

One goal of the present experiments was to elucidate the pH influence that chalcopyrite oxidation may have on the surrounding seawater during the mining of SMS deposits. Additionally, this potential for local acid generation can be viewed as a microcosm of the global issue of ocean acidification caused by dissolution of anthropogenic atmospheric CO_2 into the oceans. Because sulfide mineral oxidation rates typically increase with lower pH, any worldwide drop in ocean pH due to CO_2 dissolution may amplify the breakdown of SMS deposits, further affecting the marine ecosystem.

Constraining the oxidation rates of individual sulfide mineral species in seawater will be useful in modeling SMS mining repercussions, as well as in understanding natural chemical weathering and element cycling in the oceans over geologic time. Since chalcopyrite is relatively slow to oxidize, the data collected here provides a minimum abiotic rate of anthropogenic and natural oxidation of SMS deposits. Biotic influence on the rate can then be quantified in comparison to strictly abiotic oxidation.

MINERAL PREPARATION

Ore specimens containing large, visually pure crystals of sulfides and quartz from the Casapalca Mine in Peru were first broken up by hammer and chisel inside of a shatter box (Figure 3). Chalcopyrite and sphalerite (ZnS) were the main sulfide constituents, accompanied by trace amounts of pyrite (FeS_2) (Figure 4). The smaller shards of rock were inspected by eye and sorted visually according to chalcopyrite content. The purity of these samples was further refined by grain separation with tweezers under a binocular 3.5-90x optical microscope. Pieces too small for such manipulation were removed by sieving.

Representative samples of these purified starting materials were then analyzed by powder X-ray Diffraction (XRD) to confirm mineral identity and verify that there were no major mineralogical impurities (Figure 5). Energy Dispersive Spectroscopy (EDS) was used on the Scanning Electron Microscope (SEM) to quantify the elements present in the starting material. The sorted chalcopyrite used here was indeed relatively pure based on XRD and EDS; only a few of the surveyed grains contained small amounts of zinc (presumably from optically undetectable sphalerite impurities) or chromium (possibly from the hammer and chisel). A typical EDS spectrum of elemental composition for most of the grains analyzed is included in Figure 6.

Another application of the SEM during the preparation process was to assess the effectiveness of pre-run grain surface cleaning procedures. The cleaning procedure used was modified from McKibben and Barnes (1986) and McKibben et al. (2008). First,

chalcopyrite of desired grain size and mass was cleaned ultrasonically in acetone for 5 minutes. The dust laden acetone was then decanted to prevent clogging of the filter paper in subsequent steps. A 5-minute ethanol rinse through a vacuum filtration apparatus removed the acetone and dried the chalcopyrite before a 1M hydrochloric acid (HCl) treatment. Grains were agitated in the HCl for 20 to 30 seconds before soaking for an additional 5 minutes. The HCl was decanted prior to a final ethanol rinse and 5-minute vacuum dry. The images of Figure 7 demonstrate that this technique yields fresh reactive surfaces with minimal excess material or contamination.

Nitric acid (HNO_3) had been used first for grain surface pretreatment, but an initial spike in aqueous Cu and Fe concentrations was found during preliminary reaction runs (Figure 8). Using HCl instead of HNO_3, as described above, produces a dampened peak. One explanation for this phenomenon may be that the reaction between the acids (HNO_3 more than HCl) and chalcopyrite produces a thin layer of soluble (but not detectable by SEM) oxyhydroxides on the surface of the grains that, when exposed to seawater, immediately release a larger amount of Cu and Fe than the bulk mineral surface does itself. Another possibility is that exposure to the air after pretreatment causes a thin oxyhydroxide product layer to form (Figure 9). The composition, thickness, and behavior of such a product layer have been studied extensively (Yin et al., 2000; Vaughan et al., 2002; Goh et al., 2006). If this was the case, one would expect EDS analysis to show peaks for O, which it did not. Perhaps such peaks will not show, even if an oxide or

oxyhydroxide layer is present, if that layer is very thin or discontinuous (patchy). Previous studies do suggest the product layer to be only 1-2 nm thick (Yin et al., 2000).

The initial data spike does dissipate, though. One hypothesis to explain this observation is the formation of Cu and Fe chloride complexes on the chalcopyrite surface subsequent to the dissolution of the previously mentioned oxyhydroxide layer. Post-run EDS analyses do show Cl on the surface, but by the time the reacted, unrinsed mineral surface was analyzed in the SEM, the seawater had evaporated leaving a coating of salt that would cause a thin product layer to be indistinguishable.

Another hypothesis is that the data spike reflects a swift drop in pH upon contact between the seawater and sulfide, resulting in enhanced dissolution and increased production of sulfuric acid. That immediate reaction was buffered slowly by the synthetic seawater, made from commerical aquarium salt (Kent) whose exact composition was unknown. Unspecified buffering components included in the salt mixture by the company may have compensated for this initial drop in pH gradually enough to be captured by increased Cu and Fe concentrations but quickly enough to leave this pH change undetected. Preliminary pyrrhotite dissolution experiments (Romano and McKibben, 2011) also exhibit an initial spike when using the commercial aquarium salt mixture, but not when the matrix is formulated following Millero's (2005) synthetic seawater recipe. This discrepancy is addressed in more detail later.

Nonetheless, the importance of using cleaned grains without dust is evident from studies such as Acero et al. (2007). Their flow-through experiments continued for

months and show an initial rapid dissolution period during which the reaction was probably driven quickly by dissolution of the smaller, more abundant particles with a higher surface area to volume ratio and possibly different chemical composition, rather than by the chalcopyrite itself.

Constraining the surface area and mass of the mineral grains is necessary to derive a specific rate law for dissolution. In any fluid-mineral reaction, more available mineral surface will result in a faster reaction. So, for example, the reaction rate of 2 grams of grains having diameters between 45μm and 106μm will proceed faster than that of larger grains having diameters between 106μm and 150μm. In other words, an increase in the specific surface area of the grains (m^2/g) will lead to an increase in the rate of a reaction because there is more exposed material with which the fluid can react.

A technique used commonly to determine the specific surface area of powdered solids is called the B.E.T. method (Brunauer et al., 1938). This gas adsorption technique provides a measure of surface area per unit mass, usually given in m^2/g. For chalcopyrite, surface area was obtained both locally at the USDA Salinity Lab on the U.C. Riverside campus and commercially by Quantachrome Instruments in Boynton Beach, Florida. The B.E.T. method was used in both cases for grain diameters between 106μm and 150μm, chosen based on published sulfide kinetics research (McKibben and Barnes, 1986 and McKibben et al., 2008) and available sieves. 0.065 m^2/g was the local result while the surface area determined by Quantachrome was 0.032 m^2/g. Only a single-point nitrogen gas analysis was performed at the Salinity Lab, which probably

produced less accurate data than the 3-point krypton gas analysis done by Quantachrome. Therefore, the specific surface area value used to derive a rate law for chalcopyrite between 106µm to 150µm in was the Quantachrome value of 0.032 m^2/g.

To test the effect of surface area on reaction rate and produce dissolved Cu and Fe concentration data farther above the detection limits of the analytical techniques described below, chalcopyrite grains averaging 45µm to 106µm in diameter were also used in the present study (grains smaller than 45µm would escape the confining mesh screen of the experimental sample holder). The majority of later runs, especially under colder temperatures, high pH and low dissolved oxygen conditions (where rates are slowest) were performed using grains in this size fraction. 3-point krypton B.E.T. analysis performed by Quantachrome yielded a surface area of 0.062 m^2/g for this grain diameter range.

After confirming chalcopyrite purity, investigating the effectiveness of pre-run cleaning, and determining the grain specific surface area, the preparatory phase for chalcopyrite was complete. Details regarding how experiments were performed and reaction products were analyzed are described in the following section.

EXPERIMENTAL DESIGN

There are a handful of possible experimental approaches in geochemical kinetics, but batch (closed) and flow-through (open) reactors are used most commonly (Brantley et al., 2008). The batch design was employed to obtain the data discussed here. Flow-through experiments were considered and attempted, but abandoned due to the extremely slow rate of reaction between chalcopyrite and seawater (resulting in long run times and high reagent consumption and disposal costs).

During runs performed in batch mode, precipitates may form in solution or as a coating on the mineral surface because the seawater is not evacuating the vessel to be replaced with fresh matrix as it would in flow-through runs. Therefore, only initial reaction rates are best studied this way (Lasaga, 1998; McKibben and Barnes,1986; McKibben et al., 2008). An equation specific to analyzing data gathered during batch experiments to determine a rate law is explained and used in later sections.

Experimental Setting

For each experimental run, as many as two 2-liter Teflon batch reaction vessels were immersed in a temperature controlled bath (Figure 10). A 50/50 mixture of antifreeze and water filled the bath to avoid coolant freezing at lower temperatures and prevent corrosion of the steel bath. Also, a layer of hollow Teflon balls covering the bathwater surface served as insulation to help stabilize the temperature. Ports for input and output of seawater, sampling, a thermometer, and a fritted gas dispersion tube for gas

saturation were built into the vessel lids and unused ports were sealed to prevent atmospheric oxygen exchange (Figure 11).

Within each vessel, two parallel disks of 30 μm nylon mesh screens sandwiched 1-2 grams of the mineral grains. These disks were held taught by threaded PVC trap valve fittings screwed tightly together, similar to previous studies (e.g., McKibben and Barnes, 1986; Rimstidt and Newcomb, 1992; Williamson and Rimstidt, 1994; McKibben et al., 2008). The assembled sample platform was held suspended within the body of the vessel by three vertical Plexiglass fins. The mesh allowed synthetic seawater, made from aquarium salt and 18.2 MΩ water ("Ultrapure") in proportions akin to natural seawater, to thoroughly interact with the grains while constraining and preventing grain collisions with each other or with the vessel walls. This dual-disk grain enclosure also prevented the entrainment of mineral grains in matrix samples taken for reaction product analysis. As a modification to the set-up of previous studies, a large nitrile o-ring separated the two disks and provided enough space for the chalcopyrite to ensure that every available grain surface interacted with the circulated seawater matrix.

Desired initial pH was attained by adding aliquots of 0.1M or 1M HCl to the synthetic seawater. Salinity was held constant by adding ~34 g aquarium salt per liter of solution for every run. The composition of each batch of seawater did vary, despite an effort to use an identical recipe every time, apparently because of variability in the aquarium salt manufacturing process. Compensation was made for this variation during ICP-MS data analysis and is discussed in detail in Appendix A.

Dissolved oxygen concentrations were controlled by finely bubbling gas from 10% or 99.5% oxygen-nitrogen gas mixtures into the seawater for the duration of each experiment, using glass dispersion tubes. The prepared seawater matrix was also saturated with the same gas for no less than 45 minutes preceding the beginning of a run. Before runs below 20-25°C, the seawater was equilibrated to the desired temperature and oxygen concentration simultaneously in an additional bath.

As outlined in the previous section, grains were cleaned immediately before experimentation to expose fresh, reactive surfaces with minimal dust and oxidation products. The starting material was loaded into the sample platform, the reaction vessel and accompanying glassware were assembled, and purged/equilibrated seawater was fed into the set up as soon as the chalcopyrite was cleaned and loaded into the vessel. The time of initial contact between the matrix and mineral was considered time zero of the reaction.

Between every set of runs, equipment was cleaned meticulously. Sample platform parts and fins, tubing connectors, and the Teflon ball used to cover the sample port were placed inside the Teflon reaction vessel which was then filled with 5% HNO_3 and allowed to soak for about 24 hours. The 5% HNO_3 was removed from the vessel and all parts were rinsed with UV-irradiated Ultrapure water. The vessel still containing all previously mentioned equipment was refilled with Ultrapure water and left to soak for another 24 hours. Pipette tips were cleaned separately in the same manner and discarded after use.

All glassware used for preparation of synthetic seawater, cleaning of chalcopyrite, and as part of the experimental set up was cleaned vigorously with Alconox (a commercial detergent), Citronox (a commercial weak acid mixture), and rinsed several times with UV-irradiated Ultrapure water before each use.

Trial runs

Data from initial debugging runs were considered to determine length of experiments, cleaning technique, and the appropriate rate of fluid circulation through the vessel. Our goal was for the rate of the reaction we measure not to be controlled by the velocity of the seawater moving past the grain surfaces (ionic transport control), but by natural processes on the mineral surfaces (surface reaction control). Following McKibben et al. (2008), the flow rate was increased in a step-wise manner until the reaction ceased to increase, reflecting the point at which the transport of the fluid matrix no longer influenced the reaction rate. This minimum flow rate (440 mL/min.) was use for the subsequent experiments.

Another important factor examined during trials was the speed of fluid mixing within the reactor. Although a flow rate of 440 mL/min. reflected how fast the seawater needed to travel so that the reaction rate was based on mineral-matrix interactions, the reaction product data produced at that pump speed was undesirably unpredictable in a spatial sense within the vessel, reflecting variability in pipette insertion depth and thus the sampling practices of individuals who obtained the sample. So that sampling captured representative Cu and Fe levels within the seawater matrix and not inconsistent patches,

simple tracer tests were executed using food coloring dye (Figure 12). These tests were performed under run conditions, including placement of inflow, outflow, mixing, and gas dispersion tubes. The sample platform was also positioned in its experimental location. For the utilized Masterflex L/S Economy Drive model 07554-90 peristaltic pump and EasyLoad pump head, setting the speed to the "8" setting (corresponding to a flow rate of about 1300-1400 mL/min.) was sufficient to homogenize the content of a 2-liter vessel containing all necessary experimental equipment in about 31 seconds. A faster pump setting would be unnecessary because the time between initial contact of seawater with chalcopyrite and the first experimental sample was always longer. Keeping the pump on this lowest usable setting minimized wear on the peristaltic tubing, helping to prevent leakage and subsequent spontaneous evacuation of the reaction vessel.

Rapid mixing was also confirmed by direct measurements during batch run L30. Duplicate samples were obtained from different port locations within the reaction vessel. Figure 13 shows data from this run alongside an explanation of the duplications.

Fluid mixing was achieved with a peristaltic pump. As illustrated in Figure 14, the seawater inflow and outflow were positioned directly above and below the chalcopyrite, respectively. The proximity of the glass flow pipes to the sample platform was favorable because it guaranteed high fluid flow rates through the chalcopyrite grains. Size 24 Tygon LFL grade Masterflex tubing was ultimately chosen for the pump heads due to its durability and effectiveness. A short segment was clamped into the pump head while lower grade size 18 tubing was used on each end for a better fit over the reaction

vessel glassware. The size 24 tubing clamped inside the pump head was shifted once over the course of the run to prevent wear, always after a sample was extracted. A closed system was maintained for every experiment.

The duration of the batch experiments was another factor determined from data obtained during trials. The reaction proceeded relatively slowly, so runs about 72 hours long were preferred. Example data collected over 72 hours is included in Figures 14 and 15.

Sample Acquisition and Analysis

Fluid samples were extracted by a fixed-volume micropipette at intervals throughout each run, always more frequently in the beginning. Chemical composition was measured with an Agilent 7500 ChemStation Inductively Coupled Plasma Mass Spectrometer (ICP-MS) at the University of California, Riverside. Samples were acidified 10-fold using 2% trace metal grade HNO_3, recommended for this type of analysis. Dilution less than 10-fold would be detrimental for the ICP-MS machine due to the high salinity of the matrix. For this reason, only 1 mL was removed from the run for each sample aliquot, resulting in minimal seawater volume change over the lifetime of a run.

Standards containing known Cu and Fe concentrations and trace metal grade 2% HNO_3 were analyzed alongside run samples. Due to a high background concentration of sulfate already present in seawater, dissolved S produced from the reaction could not be

accurately quantified. Appendix A describes the calibration and calculation methods tested and used during analysis.

Use of an Inductively Coupled Plasma Optical Emission Spectrometer (ICP-OES) was tested as an alternative, but the low sample concentrations tested the detection limits of the machine for both Cu and Fe. The data were therefore unreliable.

Copper ion-specific electrode measurements were also attempted but proved not to be useful because the Cu initially present in the collected sample oxidized rapidly from exposure to the atmosphere. Concentrations measured even minutes after the sample was taken were consistently lower than they had been immediately after the sample vial had been filled. Temperature change was ruled out as a cause for this discrepancy because the concentration drop still occurred under constant temperature conditions. Use of an oxygen-free sampling and analysis system might make the use of specific ion electrodes feasible, but would greatly complicate the experimental and analytical procedures.

REACTION STOICHIOMETRY AND RATE-INDICATING VARIABLES

The dissolution of chalcopyrite examined in this study was not stoichiometric under all conditions. Generally, the reaction behaved congruently when pH <4.0, P_{O_2} was low, and/or the temperature was around or below 10°C (Figure 15). If dM_{CuFeS_2}/dt is defined as the molar rate of oxidation, its sign is negative since the mineral was destroyed. Hence, the molar rate of release of Cu ($dM_{Cu(aq)}/dt$), Fe, ($dM_{Fe(aq)}/dt$), and SO_4 ($dM_{SO4(aq)}/dt$) have positive values. A stoichiometric dissolution reaction can be expressed by the following relationship:

$$- dM_{CuFeS2}/dt = dM_{Cu(aq)}/dt = dM_{Fe(aq)}/dt = 0.5dM_{SO4(aq)}/dt$$

Each mole of chalcopyrite that dissolves yields one mole of $Cu_{(aq)}$ and $Fe_{(aq)}$ plus two moles of $SO_{4(aq)}$, so that the sulfate release rate is twice that of the Fe and Cu rates. On the other hand, if the reaction is incongruent, the rates of the products may not be correlated in this way. In this case, one or more constituents are forming precipitates or remaining behind as unreleased solid phases instead of becoming ions in solution. This phenomenon occurred at pH ≥ 4.0.

If one product element (Fe or Cu) precipitated, i.e. as stain on the mesh or as clouded pump tubing at the end of a run, the other was chosen as the rate-indicating metal. At pH < 4.5, Cu was selected as the rate-determining variable.

RESULTS

78 batch experiments were conducted for this project; a detailed description of those incorporated into the rate law can be found in Appendix B. Run data used to compute the reaction orders and rate constant of the equation were chosen based on reproducibility. It should be noted that partial pressures of oxygen (P_{O2}) were used to derive the rate because they were known directly with confidence. Calculations to convert P_{O2} to dissolved O_2 concentrations in seawater are outlined in the discussion section alongside a proposed equivalent rate law. The molal specific rate law (moles kg^{-1} m^{-2} sec^{-1}) for the oxidation of chalcopyrite in seawater is:

$$R_{sp} = - 10^{-9.38}(P_{O2})^{1.22}(H^+)^{0.36}$$

Formation of precipitates

Batch runs at P_{O2} = 0.995 atm were executed with acidic seawater to avoid precipitation of Cu and Fe hydroxides and chlorides. Fe precipitates appeared as rust-colored stains on the nylon screens above pH 4 (Figure 16) while the white solids that formed in experiments at unaltered seawater pH (~8.2) were presumed to be Cu precipitates due to their appearance (i.e. not rust colored) (Figure 17) and known conditions of Cu complex formation in seawater (e.g. Hannington, 1993).

In an effort to suppress precipitation long enough to obtain a usable rate at higher pH values, a few runs were performed under a lower P_{O2} using a 10% O_2 gas mixture balanced with N_2. As seen in Figure 17, a fine grained gray-white material developed on the mesh and inner walls of the pump tubing after about one day. Plots of Cu and Fe

concentrations over time (Figure 18), show that neither Cu nor Fe appear to remain in solution as ions or free-floating precipitates and the initial release rates of both metals were essentially zero at pH 8. Erratic data produced from such runs that resulted in precipitation hindered computation of an initial rate.

Rate dependence on P_{O2} and proton concentration

The effect of P_{O2} on the rate was tested from 0.10 atm to 0.995 atm, at 21.0°C to 23.5°C, and pH 3.0±0.2. Reaction orders for P_{O2} calculated as the slopes of the solid and dashed lines fit to Fe and Cu data, respectively, in Figure 19 are: Fe: 0.0057±0.6826, Cu: 1.216±0.1107. pH reaction orders computed similarly are: Fe: -0.1226 ±0.2776 Cu: 0.3633±0.09. Figure 20 illustrates the rate dependence on proton concentration for low pH, 21.0°C to 23.5°C, and high P_{O2}.

Temperature and surface area effects on oxidation

The reaction was faster at higher temperatures (Figure 21), as predicted by thermodynamics and previous studies (Acero et al., 2007; Kimball et al., 2011). The activation energy (E_a), calculated from the Arrhenius Plot in Figure 21, is ~10.14 kJ/mol.

DISCUSSION

Using a laboratory approach to study water-rock interactions, a rate law was formulated to express the oxidation of chalcopyrite in seawater. To derive the rate law, the initial rate method (Lasaga, 1998) was combined with the isolation method, as practiced and described by McKibben and Barnes, 1986 and McKibben et al., 2008. A second-order polynomial equation (see Appendix B) was fit to all data because the rate of release of both Cu and Fe decreased over time. Initial rates were obtained by regression for pH 2.2-4.5. For this pH range, Fe precipitation was observed above pH 4.0, so dissolved Cu concentration was the rate-determining variable.

Total dissolved Fe and Cu values were typically relatively low (only up to the tens of ppb), demonstrating that the abiotic oxidation rate of chalcopyrite in seawater under conditions explored here is much lower than that of pyrrhotite (Romano and McKibben, 2011) and will thus establish a lowermost bound for the rate of oxidation of SMS deposits.

Stoichiometry of the reaction

It is possible that the congruency of the reaction observed under low temperatures, low P_{O_2}, and/or low pH (Figure 15A,B) was an artifact of how slowly the reaction took place. At conditions conducive to faster rates, the Fe and Cu rates do differ (Figure 15C).

Oxidation by dissolved O_2

The release rate of dissolved Fe is more sensitive to P_{O2} than that of Cu (Figure 19). At higher P_{O2}, Fe is released considerably slower than is Cu. Perhaps Fe is released and reprecipitated away from the surface of the mineral grains, but no such particulates were observed. Another possibility is that some Fe remains behind on the mineral surface as Cu is released, similar to non-stoiciometric behavior observed in other sulfides (McKibben et al., 2008). From low to high P_{O2}, the release rate of Cu only changes subtly. This behavior is consistent with other studies that describe O_2 concentration as a secondary rate determining factor, although they evaluated Fe(III) as the oxidant (Kimball et al., 2010). The effect of Fe(III) on the oxidation rate was not determined in the present study.

Dissolved O_2 concentrations are more complicated to calculate in seawater than pure water due to the "salting-out" effect (Benson and Krause, 1984; Garcia and Gordon, 1992). Since such saline waters contain so many dissolved constituents, there is essentially less room available for dissolved gases. Inconsistencies with temperature have also been found (Benson and Krause, 1984). The Henry's law coefficient is therefore nonlinear with both salinity and temperature. For more accurate comparison with previous research, dissolved O_2 concentrations were calculated using a modified version of the following equation from Benson and Krause (1984), tested by Garcia and Gordon (1992) and evaluated and recommended by Wong and Li (2009):

$$C_o^* = 0.20946\, F\, (1 - P_{wv})\, (1 - B_o)\, (K_o M_w)^{-1}$$

where P_{wv} is the water vapor pressure in air, M_w is the gram molecular mass of water, and 0.20946 is the mole fraction of O_2 in dry air. The salinity factor, *F*, is defined in Benson and Krause's 1984 paper but based on Millero (1982). B_o is the second virial coefficient for O_2 from Benson and Krause (1980). K_o is the Henry's coefficient for O_2 in seawater based on measurements made by Benson and Krause (1984).

Since the partial pressure of O_2 was known for each run, that value was substituted for the coefficient describing the mole fraction of O_2:

$C_o^* = 0.10\ F\ (1 - P_{wv})\ (1 - B_o)\ (K_oM_w)^{-1}$ for the 10% O_2 gas mixture, and

$C_o^* = 0.995\ F\ (1 - P_{wv})\ (1 - B_o)\ (K_oM_w)^{-1}$ for the 99.5% O_2 mixture.

Calculations were performed with varied chlorinities to investigate the effect of the salinity factor, *F*, on C_o^*. Millero (1982) recommends a salinity range 33-37, so computations were made for each end of the spectrum to be sure the change in *F* was negligible.

Values of C_o^* were published in Benson and Krause (1984) in mol/L at integral temperatures and salinity intervals of five. A salinity of 35 was chosen because it was the closest to our synthetic seawater recipe. Since these tabulated values considered an atmosphere containing 20.946% O_2, they were converted to the experimental conditions of 10% O_2 and 99.5% O_2 by simple division and multiplication. Table 1 below contains the C_o^* for each temperature investigated.

The dissolved O_2 concentration should be in mol/kg for the rate law, compiled in Table 2. $C_o^\dagger$ is given as µmol/kg and Equation 23 in Benson and Krause (1984) relates C_o^* to $C_o^\dagger$ by density:

$$C_o^* = \rho_s C_o^\dagger$$

Table 1: Published C_o^* modified for these experimental conditions.

Temperature (°C)	Salinity	C_o^* (mg/L) from Benson and Krause (1984)	$P_{O_2} = 0.10$	$P_{O_2} = 0.995$
7.0	35	9.647	4.606	45.826
8.0	35	9.431	4.503	44.800
9.0	35	9.223	4.403	43.812
10.0	35	9.024	4.308	42.867
20.0	35	7.396	3.531	35.133
21.0	35	7.262	3.467	34.497
22.0	35	7.134	3.406	33.889
23.0	35	7.009	3.346	33.295
24.0	35	6.888	3.288	32.720
25.0	35	6.771	3.233	32.164

Table 2 shows the dissolved O_2 concentrations used in this version of the law, after correcting for seawater density and converting from µmol/kg to mol/kg.

Table 2: Molal concentrations of dissolved O_2 based on values published in Benson and Krause (1984).

Temperature (°C)	$C_o^\dagger$ (µmol/kg) from Benson & Krause (1984)	$C_o^\dagger$ (µmol/kg) for $P_{O_2} = 0.10$	$C_o^\dagger$ (mol/kg) for $P_{O_2} = 0.10$	$C_o^\dagger$ (µmol/kg) for $P_{O_2} = 0.995$	$C_o^\dagger$ (mol/kg) for $P_{O_2} = 0.995$
7.0	293.44	140.094	0.000140	1393.931	0.001394
8.0	286.91	136.976	0.000137	1362.912	0.001363
9.0	280.93	134.121	0.000134	1334.505	0.001335
10.0	274.61	131.104	0.000131	1304.483	0.001304
20.0	225.54	107.677	0.000108	1071.385	0.001071
21.0	221.53	105.762	0.000106	1052.336	0.001052
22.0	217.67	103.920	0.000104	1034.000	0.001034
23.0	213.92	102.129	0.000102	1016.186	0.001016
24.0	210.30	100.401	0.000100	998.990	0.000999
25.0	206.79	98.725	0.000099	982.317	0.000982

Figure 19B is a plot of the rate dependence on dissolved O_2 estimated from calculations made using values and equations in Benson and Krause (1984). The adjusted rate law in moles kg^{-1} m^{-2} sec^{-1} is:

$$R_{sp} = - 10^{-9.38}(D.O.)^{1.62}(H^{+})^{0.36}$$

Rate dependence on pH

Cu was released into solution noticeably slower with less acidity from pH 2.2 to 4.0 (Figure 20). Overall, seawater pH did not drop noticeably over the course of every experiment. For example, one run starting at pH 4.0 (L69) and another starting at 4.1 (L70) dropped to about 3.7 and 3.8, respectively, by the end of the runs. As expected, a drop in pH over time was observed during runs at pH 4.0 and 4.5, but not at lower pHs. The higher initial concentration of protons at more acidic conditions most likely does not allow for a detectable effect on pH.

Temperature and surface area effect on oxidation

In these experiments, there was a positive correlation between reaction rate and temperature. The activation energy (E_a), calculated from the Arrhenius Plot in Figure 21, is lower than what has been obtained in previous works (Lin and Sohn, 1987; Acero et al., 2007; Kimball et al., 2010): ~10.14 kJ/mol. It is possible that low pH and higher Cl^- content have a significant enough impact on E_a to produce this discrepancy. As mentioned earlier, publications including Lu et al., 2000; González-Dávila et al., 2009; and Ruiz et al., 2011 do hypothesize that Cl^- ions accelerate this reaction.

Few runs under low specific surface area conditions gave a measurable initial rate. It was expected that more surface area would create a higher rate. For this work, a grain size smaller than 45μm to 106μm to produce more available reactive surface was impossible. The mineral would have escaped the mesh screen intended to retain it during the batch runs. Crushing and cleaning more mass was also not preferable due to the crowded nature of the sample holder. Data collected from preliminary runs using grains one size fraction larger (106μm to 150μm) did not provide a discernible rate that could be used with confidence.

Despite a lack of extensive empirical data to demonstrate the surface area effect on the oxidation of chalcopyrite in seawater, the literature (i.e. Kimball et al., 2010) helps maintain the prediction that a higher surface area to volume ratio will escalate the rate of this reaction.

Implications for seafloor mining

The slow pace of this reaction is encouraging for the prospect of seafloor mining. Sulfuric acid production from the oxidation of chalcopyrite alone will probably not play a dominant role in significantly changing the pH of waters surrounding seafloor mines. Assuming stoichiometric oxidation of 1 mole of chalcopyrite, 1 mole of protons would be released (Equation 2). Therefore, the oxidation of 1 kg of chalcopyrite would only produce 0.482 kg of protons. Nautilus Minerals Inc., completed elutriate tests that determined that waste water would need to be diluted 4000 times in order to meet water quality requirements. Their tests incorporated material taken directly from the future

mine site rather than individual sulfides, implying that dissolution of other minerals (i.e. pyrite, galena, etc.) will probably produce much of the acid responsible for shifting seawater pH that drastically.

Furthermore, only a small amount of copper was released into solution relative to the starting material, an economically favorable situation for maximizing metal recovery during slurry transport to surface ships. SEM images show a lack of dramatic mineral surface alteration, unlike some previous studies on other sulfides (Avery and Benning, 2008; McKibben et al. 2008). Preservation of mineral surfaces is also economically promising.

Preliminary data on rates of pyrrhotite oxidation (Romano and McKibben, 2011) suggest that this iron monosulfide mineral oxidizes more quickly in seawater than chalcopyrite and may have a more significant effect on local acid production during mining of SMS deposits. Even so it is plausible that the sulfuric acid created from *in situ* mining of SMS deposits will not exceed the buffer capacity of local seawater, even on a human time scale. The buffer capacity of seawater (B_c) can be related to the chlorinity by the following equation:

$$B_c/Cl = 0.1252 \text{ (Thompson and Bonnar, 1931)}$$

If average seawater contains about 34 g of salt per kg of seawater including about 19 g of Cl^-, the B_c will be about 2.38 g of acid per kg of seawater. As mentioned earlier, if congruent oxidation of chalcopyrite occurs following equation 2 then 1 mole, or 1.008

grams, of acid is produced. This is well within seawater's buffer capacity, especially factoring in advective effects.

The ore processing waste that will be injected into the water column from surface ships will have a high amount of freshly reactive surface area: the grains will average <8μm in diameter (Nautilus, 2008d). Experimental inquiries assessing acid generation from a "return plume" of such finer grained sulfides to supplement existing modeling data would be very useful for designing mitigation plans. However, ignoring for a minute the immediate localized effects of introducing acidic water to the Bismarck Sea, it seems that the sheer volume of water in the sea will couple with B_c to dilute, disperse, and buffer the acid produced.

The data presented here indicate that aging, weathering SMS deposits will become relatively enriched in Cu if chalcopyrite does oxidize slower than other sulfides found in these settings (e.g. pyrite, pyrrhotite). As the other minerals dissolve more quickly, the Cu/Fe ratios increase over time. This process is additionally applicable to VMS deposits which currently provide a significant amount of Cu and Au worldwide. Weathered hydrothermal vent and mound material is tectonically buried, obducted and preserved in continental rock as a VMS deposit. Cu/Fe ratios in SMS deposits vary: 0.18 in volcanic-hosted deposits at ocean ridges, 0.28 at intra-continental back-arc spreading axes, and 0.38 at intra-oceanic back-arcs (Rona, 2008). These values can be compared to slightly higher values of the same ratios in VMS deposits: 0.48 and 0.21 in the upper and lower black ore/sulfide zones, respectively (Franklin et al., 1981). Understanding the

history of these resources during their formation and subsequent natural dissolution in seawater can be instrumental in identifying future resources.

FUTURE WORK

Environmentally, the most vital information regarding SMS mining is how the ocean environment is going to be impacted. Fresh sulfide mineral surfaces and potentially harmful acid will be introduced to the system in unnatural quantities on an expedited timescale that may create unnatural and unfavorable results.

To more accurately gauge the potential for pH shifts caused by sulfide oxidation, commercial aquarium salt is not recommended for use as synthetic seawater for kinetic experiments. Initially, the efficiency of using pre-mixed salts to emulate ocean water made it an attractive idea. Batch to batch inconsistency of the salt was unfavorable. Analytical methods were adjusted to make up for the minor variations in the elemental composition (Appendix A) but the artificial solutions were otherwise uniform: the addition of a predetermined amount of 0.1M HCl to 2 liters of solution would achieve an anticipated change in pH. Late in the progress of this research, after the purchase of more commercial salts from the same manufacturer, the pH of the synthetic seawater solution no longer responded to the added HCl as it had before. A larger volume of more concentrated (1M) acid was necessary to make comparable pH modifications. Presumably, the company added more Ca and Mg complexes to enhance the buffer capacity of the mixture, to protect aquarium fish from accidental acidification by consumers. This may have caused the anomalous initial spike in dissolved Cu and Fe values, as the buffers responded (slowly) to counter the acidity production. For future

work, the use of the fixed-composition synthetic seawater recipe of Millero (2005) is recommended.

Evaluation of the kinetics of other sulfides in seafloor settings will fuel the forecast of seafloor mining consequences as well as supplement existing knowledge of chemical cycling in marine systems. Research on the oxidation of pyrrhotite in seawater is ongoing and will provide an upper limit for the rate of the oxidative decomposition of modern and ancient sulfide-rich hydrothermal vents.

Future work should ideally also explore temperatures significantly higher than 25°C, applicable to mining localities near active vents as well as natural weathering processes of active black smokers.

CONCLUSIONS

Gaps in the kinetic literature exist concerning rate laws governing sulfide oxidation in offshore environments. Unconventional mineral resources like SMS deposits may soon be an integral component of the mining industry. Ocean acidification exacerbated by the dissolution of anthropogenic CO_2 in surface waters is also an imminent issue, mirrored by the localized acidity problem potentially caused by seafloor sulfide mining.

While there is still much work required to refine the rate laws of sulfide oxidation in seawater, data from this study of chalcopyrite in acidic seawater at low temperatures inspires several preliminary conclusions:

1) The abiotic rate of oxidation of chalcopyrite in seawater is slow and more dependent on P_{O2} than pH, but the reaction can occur more than an order of magnitude quicker at pH 2.2 than at 4.5.
2) Anthropogenic reduction of oceanic pH by rising atmospheric CO_2 (increased acidification) will therefore accelerate the weathering of SMS deposits as the condition persists.
3) At average seawater pH (~8.2), the reaction was so sluggish that the rate was considered zero. This is encouraging for mining companies looking to exploit deposits principally composed of chalcopyrite and located *away* from the influence of acidic black smoker plumes.

4) The rate of this reaction can be considered a minimum threshold for the abiotic oxidative alteration of SMS deposits and implies that natural seafloor weathering processes should result in preserved VMS deposits with higher Cu/Fe ratios, because Fe sulfides will oxidize and weather faster than Cu-Fe sulfides.
5) Acidity produced by the oxidation of chalcopyrite may be naturally buffered by the seawater, especially if the reaction behaves according to equation 2.

REFERENCES

Acero P., Cama J. and Ayora C. (2007) Kinetics of chalcopyrite dissolution at pH 3. *European Journal of Mineralogy* **19**, 173-182.

Antonijevic, M.M. and G.D. Bogdanovic (2004) Investigation of the leaching of chalcopyrite ore in acidic solutions. *Hydrometallurgy* **73**, 89-97.

Antonijevic M.M., Jankovic Z.D. and Dimitrijevic M.D. (2004) Kinetics of chalcopyrite dissolution by hydrogen peroxide in sulphuric acid; *Hydrometallurgy*, **71**, 329-334.

Avery E.R. and Benning L.G. (2008) Anaerobic pyrite oxidation rates determined via direct volume-loss measurements: a Vertical Scanning Interferometric approach. *Mineralogical Magazine* **72**, 15-18.

Benson B.B. and Krause D., Jr. (1984) The concentration and isotopic fractionation of oxygen dissolved in freshwater and seawater in equilibrium with the atmosphere. *Limnology and Oceanography*; **29**, 620-632.

Brantley S.L., Kubicki J.D. and White A.F., eds. (2008) *Kinetics of Water-Rock Interaction*. New York: Springer Science+Business Media, LLC.

Brunauer S., Emmett P.H. and Teller E. (1938) Adsorption of Gases in Multimolecular Layers. *Journal of the American Chemical Society* **60**, 309-319.

Caldeira C.L., Ciminelli V.S.T., Dias A. and Osseo-Asare K. (2003) Pyrite oxidation in alkaline solutions: nature of the product layer. *International Journal of Mineral Processing* **72**, 373-386.

Córdoba E.M., Muñoz J.A., Blázquez M.L., Gonzáalez F. and Ballester A. (2009) Comparative kinetic study of the silver-catalyzed chalcopyrite leaching at 35 and 68°C. *International Journal of Mineral Processing* **92**, 137-143.

Dove P.M. and Crerar D.A. (1990) Kinetics of quartz dissolution in electrolyte solutions using a hydrothermal mixed flow reactor. *Geochimica et Cosmochimica Acta* **54**, 955-969.

Edmond J.M., Measures C., Mangum B., Grant B., Sclater F.R., Collier R., Hudson A., Gordon L.I. and Corliss J.B. (1979) On the Formation of Metal-Rich Deposits at Ridge Crests. *Earth and Planetary Science Letters* **46**, 19-30.

Edmond J.M., Von Damm K.L., McDuff R.E. and Measures C.I. (1982) Chemistry of hot springs on the East Pacific Rise and their effluent dispersal. *Nature* **297**, 187-191.

Franklin J.M., Lydon J.W. and Sangster D.F. (1981) Volcanic-associated massive sulfide deposits. *Economic Geology 75th Anniv. Vol*., 485–627.

Garcia H.E. and Gordon L.I. (1992) Oxygen solubility in seawater: Better fitting equations; *Limnology and Oceanography* **37**, 1307-1312.

German C.R., Baker E.T. and Klinkhammer G. (1995) Regional Setting of Hydrothermal Activity. In Hydrothermal Vents and Processes, Geological Society Special Publication, No. 87.

Goh S.W., Buckley A.N., Lamb R.N., Rosenberg R.A. and Moran D. (2006) The oxidation states of copper and iron in mineral sulfides, and the oxides formed on initial exposure of chalcopyrite and bornite to air. *Geochimica et Cosmochimica Acta* **70**, 2210-2228.

González-Dávila M., Santana-Casiano J.M., González A.G., Pérez N. and Millero F.J. (2009) Oxidation of copper (I) in seawater at nanomolar levels. *Marine Chemistry* **115**, 118-124.

Hannington M.D. (1993) The Formation of Atacamite During Weathering of Sulfides on the Modern Seafloor. *Canadian Mineralogist* **31**, 945-956.

Hannington M.D., Tivey M.K., Larocque A.C.L., Petersen S. and Rona P.A. (1995) The Occurence of Gold in Sulfide Deposits of the TAG Hydrothermal Field, Mid-Atlantic Ridge. *Canadian Mineralogist* **33**, 1285-1310.

Kimball B.E., Rimstidt J.D. and Brantley S.L. (2010) Chalcopyrite dissolution rate laws. *Applied Geochemistry* **25**, 972-983.

Lasaga, A.C. (1998) Kinetic Theory in the Earth Sciences. Princeton, New Jersey: Princeton University Press.

Lin H. and Sohn H. (1987) Mixed-control kinetics of oxygen leaching of chalcopyrite and pyrite from porous primary ore materials. *Metallurgical and Materials Transactions B* **18**, 497-503.

Lu Z.Y., Jeffrey M.I. and Lawson F. (2000) The effect of chloride ions on the dissolution of chalcopyrite in acidic solutions. *Hydrometallurgy* **56**, 189-202.

McKibben M.A. and Barnes H.L. (1986) Oxidation of pyrite in low temperature acidic solutions: Rate laws and surface textures. *Geochimica et Cosmochimica Acta* **50**, 1509-1520.

McKibben M.A., Tallant B.A. and del Angel J.K. (2008) Kinetics of inorganic arsenopyrite oxidation in acidic aqueous solutions. *Applied Geochemistry* **23**, 121-135.

Mielke R.E., Pace D.L., Porter T. and Southam G. (2003) A critical stage in the formation of acid mine drainage: Colonization of pyrite by *Acidithiobacillus ferroxidans* under pH-neutral conditions; *Geobiology* **1**, 81-90.

Millero, F.J. (2005) Chemical Oceanography, Third Edition. CRC Press.

Nautilus Minerals Inc., News Release, July 10, 2007: "Significant Massive Sulphide Drill Intercepts Solwara 1." http://www.nautilusminerals.com/i/pdf/2007-07-11_NR.pdf.

Nautilus Minerals Niugini (2008a) Environmental Impact Statement: Solwara 1 Project. Volume A: Main Report.

Nautilus Minerals Niugini (2008b) Environmental Impact Statement: Solwara 1 Project. Volume B: Appendices 1-3.

Nautilus Minerals Niugini (2008c) Environmental Impact Statement: Solwara 1 Project. Volume B: Appendices 4-7.

Nautilus Minerals Niugini (2008d) Environmental Impact Statement: Solwara 1 Project. Volume B: Appendices 8-15.

Nesse W. D. (2004) Introduction to Optical Mineralogy, 3rd Edition. Oxford University Press: New York.

Parson L.M, Walker C.L. and Dixon D.R., eds. (1995) Hydrothermal Vents and Processes. Geological Society Special Publication No. 87.

Pašava J., Vymazalová A., Petersen S. and Herzig P. (2004) PGE distribution in massive sulfides from the PACMANUS hydrothermal field, eastern Manus basin, Papua New Guinea: implications for PGE enrichment in some ancient volcanogenic massive sulfide deposits. *Mineralium Deposita* **29**, 784-792.

Perry D.L., ed. (1990) Instrumental Surface Analysis of Geologic Materials. New York, New York: VCH Publishers, Inc.

Pirajno F. (2009) Hydrothermal Processes and Mineral Systems. Springer Science.

Rimstidt J.D. and Dove P.M. (1986): Mineral/solution reaction rates in a mixed flow reactor: Wollastonite hydrolysis. *Geochimica et Costmochimica Acta* **50**, 2509-2516.

Rimstidt J.D., Chermak J.A. and Gagen P.M. (1993) Rates of Reactions of Galena, Sphalerite, Chalcopyrite, and Arsenopyrite with Fe(III) in Acidic Solutions. In Environmental Geochemistry of Sulfide Oxidation, ACS Symposium Series; American Chemical Society: Washington, DC.

Rimstidt J. D. and Newcomb W.D. (1993) Measurement and analysis of rate data: The rate of reaction of ferric iron with pyrite. *Geochimica et Cosmochimica Acta* **57**, 1919-1934.

Rio Tinto (2011) Kennecott Utah Copper. 4 April 2011. <http://www.kennecott.com/>.

Robb, L. Introduction to Ore-forming Processes. Blackwell Science Ltd: Oxford, 2005.

Roberts, R.G. and P.A. Sheahan, eds. (1988) Ore Deposit Models. Ottawa, Ontario; Geological Association of Canada.

Romano G. and M.A. McKibben M.A. (2011) Kinetics of Pyrrhotite Oxidation in Seawater: Implications for Mining Seafloor Hot Spring. Geological Society of America *Abstracts with Programs* **43**(5) , 124.

Rona P.A., Klinkhammer G., Nelsen T.A., Trefry J.H., and Elderfield H. (1986) Black smokers, massive sulphides and vent biota at the Mid-Atlantic Ridge. *Nature* **321**, 33-37.

Rona P.A. (2008) The changing vision of marine minerals. *Ore Geology Reviews* **33**, 618-666.

Ruiz M.C., Montes K.S., and Padilla R. (2011) Chalcopyrite leaching in sulfate-chloride media at ambient pressure. *Hydrometallurgy* **109**, 37-42.

Shanks, W. C., III, ed. (1984) Cameron Volume on Unconventional Mineral Deposits. Hoboken, NJ; American Institute of Mining, Metallurgical, and Petroleum Engineers, Inc.

Vaughan D.J., Pattrick R.A.D. and R.A. Wogelius (2002): Minerals, metals and molecules: ore and environmental mineralogy in the new millennium; *Mineralogical Magazine*, vol. 55, pp. 653-676.

Vaughan, D.J., K.E.R. England, G.H. Kelsall, Q. Yin (1995): Electrochemical oxidation of chalcopyrite ($CuFeS_2$) and the related metal-enriched derivatives $Cu_4Fe_5S_8$, $Cu_9Fe_9S_{16}$, and $Cu_9Fe_8S_{16}$; *American Mineralogist*, vol. 80, pp. 725-731.

Von Damm K.L., Edmond J.M., Measures C.I. and Grant B. (1985) Chemistry of submarine hydrothermal solutions at Guaymas Basin, Gulf of California. *Geochimica et Cosmochimica Acta* **49**, 2221-2237.

Walker F. P., Schreiber M.E. and Rimstidt J.D. (2006) Kinetics of arsenopyrite oxidative dissolution by oxygen. *Geochimica et Cosmochimica Acta* **70**, 1668-1676.

Williamson M. A. and Rimstidt J.D. (1994) The kinetics and electrochemical rate-determining step of aqueous pyrite oxidation. *Geochimica et Cosmochimica Acta* **58**(24),5445-5454.

Wong G.T.F. and Li K. (2009) Winkler's method overestimates dissolved oxygen in seawater: Iodate interference and its oceanographic implications; *Marine Chemistry* **115**, 86-91.

Yamazake T. (2002) Development of Technical and Economical Examination Method for Cobalt-rich Manganese Crusts. International Offshore and Polar Engineering Conference, May 2002.

Yin Q.H., Vaughan D.J., England K.E.R., Kelsall G.H. and Brandon N.P. (2000) Surface Oxidation of Chalcopyrite ($CuFeS_2$) in Alkaline Solutions. *Journal of the Electrochemical Society* **147**, 2945-2951.

Yin Q., Kelsall G.H., Vaughan D.J. and England K.E.R. (1995) Atmospheric and electrochemical oxidation of the surface of chalcopyrite ($CuFeS_2$). *Geochimica et Cosmochimica Acta* **59**, 1091-1100.

FIGURES

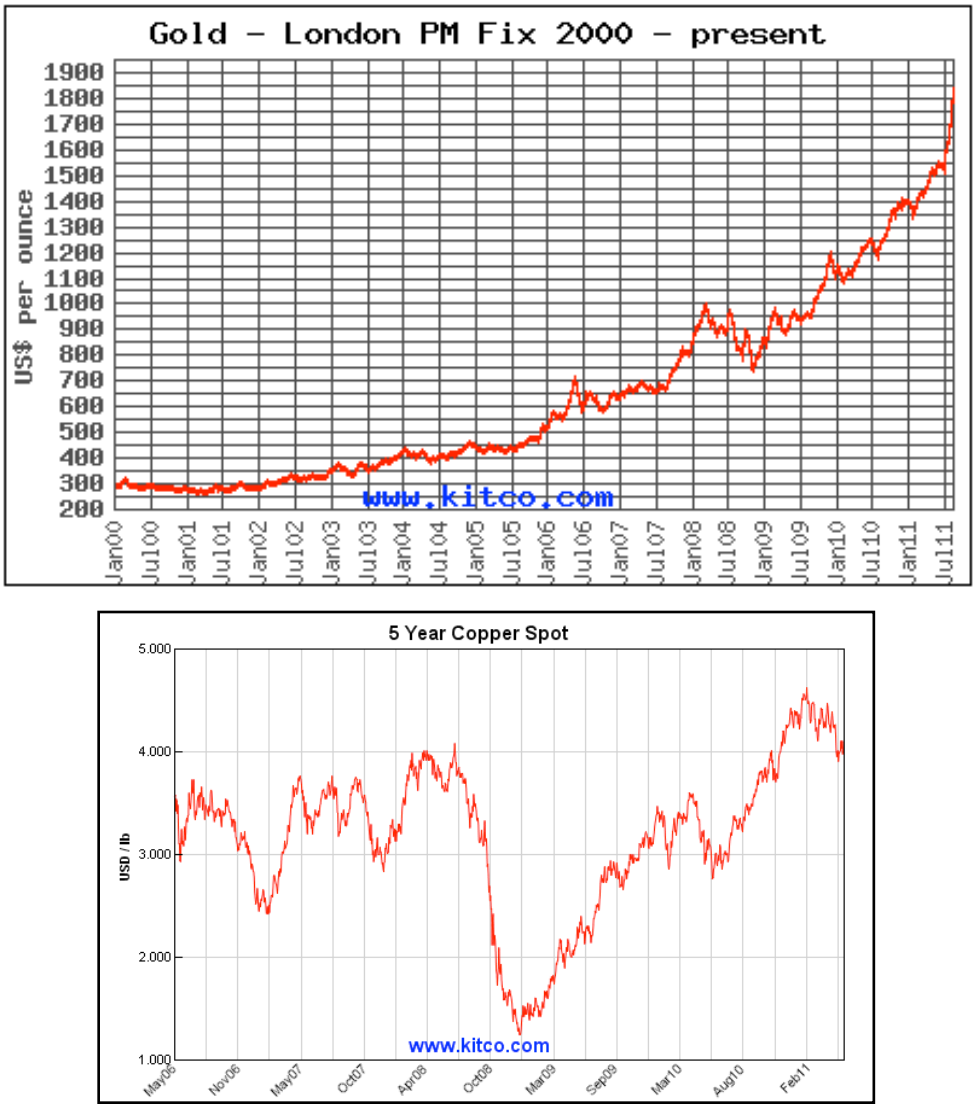

Figure 1: The fluctuation of the price of gold and copper over time (Kitco Metals, Inc., 2011).

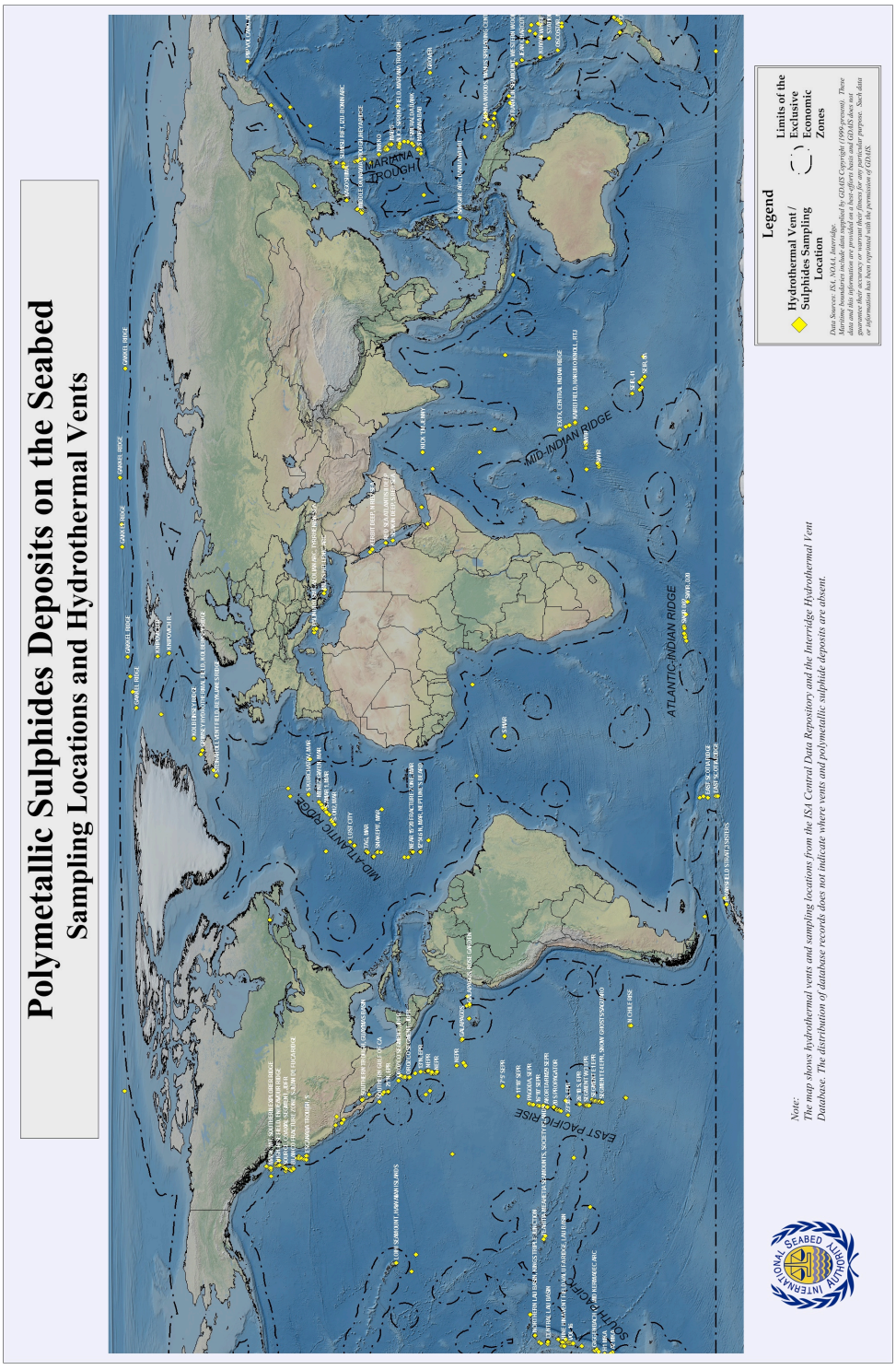

Figure 2: Exclusive Economic Zones (EEZs) encompass SMS deposits (small yellow dots) all over the globe. (International Seabed Authority, 2011).

Figure 3: Crushing station with hammer and chisel inside a protective box.

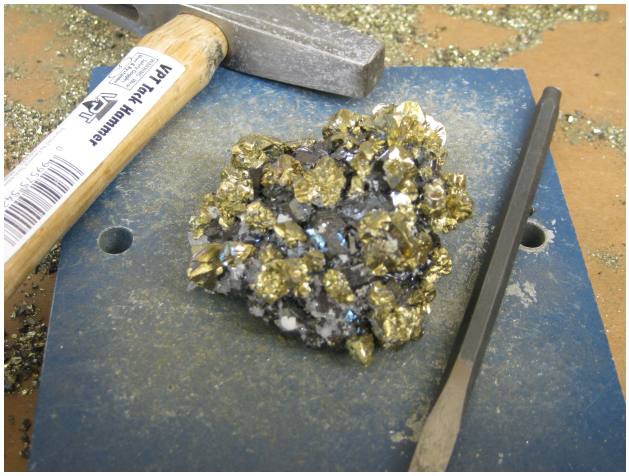

Figure 4: Chalcopyrite on sphalerite from the Casapalca Mine, Peru.

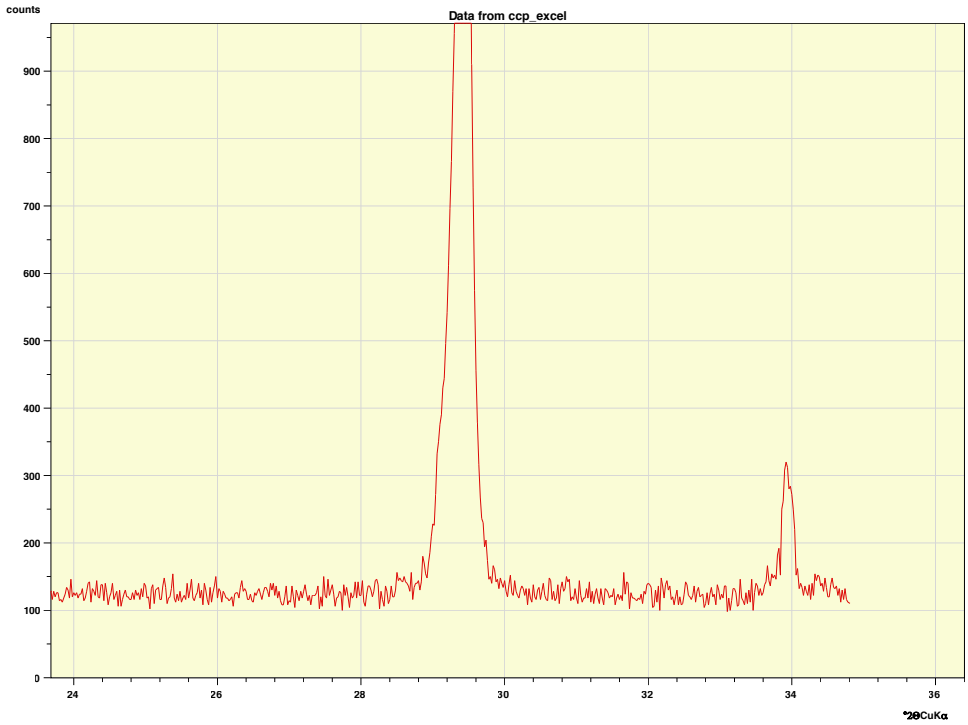

Figure 5: This plot of 2-theta versus counts from XRD data of chalcopyrite shows two dominant peaks with minimal impurity. X-axis is 2θCuKα from 23.6 to 36.4, y-axis represents counts from 0 to 975.

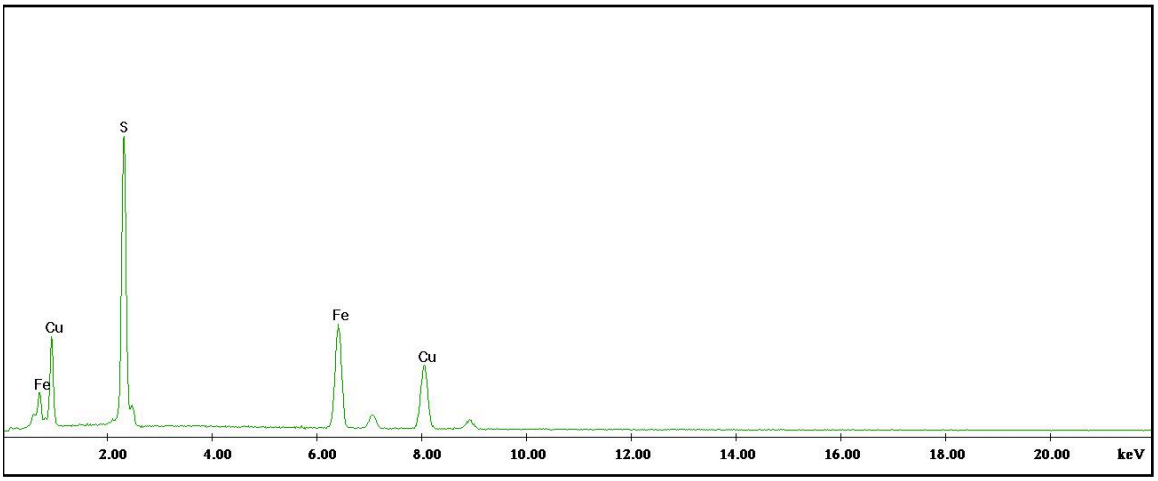

Figure 6: EDS data showing Cu, Fe, and S are the main constituents of the chalcopyrite obtained from Peruvian samples. X-axis shows keV and peaks should be considered relative to one another.

(A)

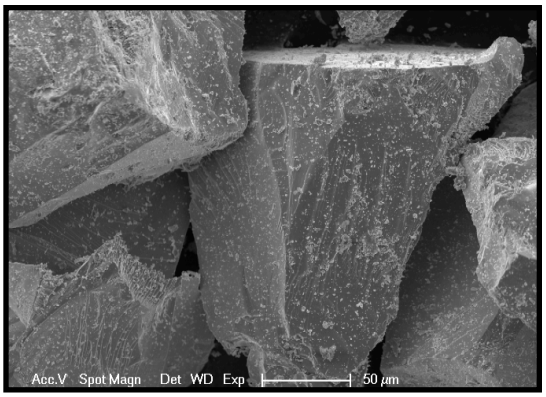

(B)

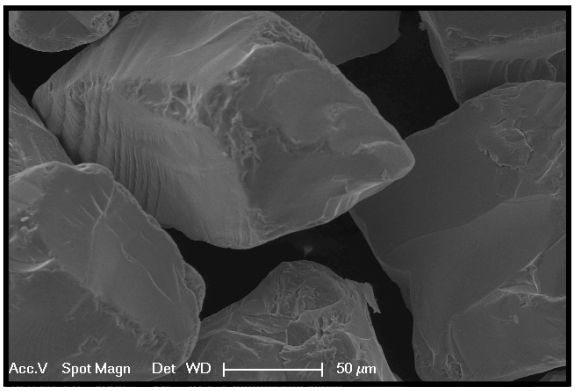

Figure 7: (A) 106µm to 150µm size chalcopyrite grains without cleaning; (B) Chalcopyrite grains after full treatment. Grain surfaces in image A contain many smaller particles, compared to the smooth, dust-free surfaces in image B.

Figure 8 (charts on following page): (A) Trial batch run L16, performed at 20°C in pH 3 seawater, shows Fe concentrations to be higher immediately after the start of the reaction than they were in the blank matrix with the chalcopyrite cleaned for 5 minutes in 1M HNO_3. (B) Fe concentrations spike even higher when the grains soaked longer in 1M HNO_3. (C) When cleaned for 5 minutes in HCl instead, the initial peak was not as prominent. In graphs A, B, and C, the background seawater was not subtracted from the data so that the Fe and Cu data were separated on the plot for easier interpretation.

L16: 5-minute 1M HNO_3 soak

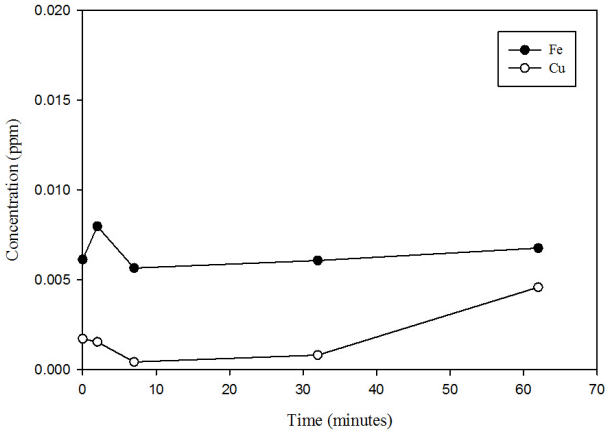

(A)

L18: 20-minute 1M HNO_3 soak

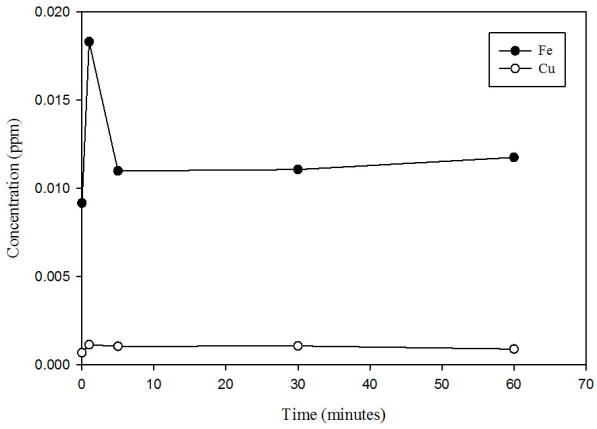

(B)

L17: 5-minute 1M HCl soak

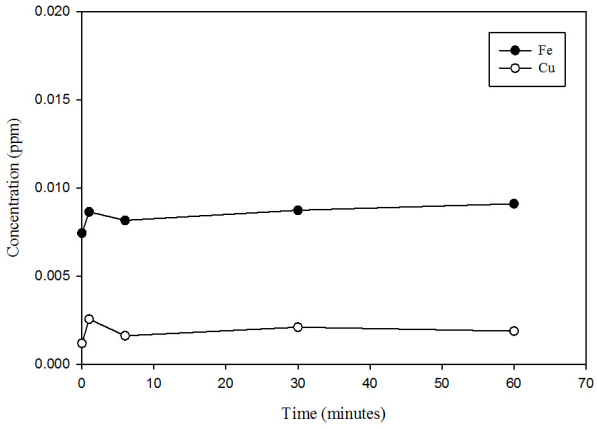

(C)

Figure 8 (Caption on previous page).

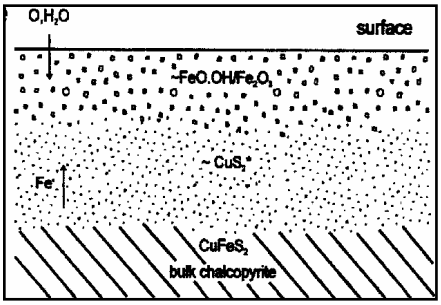

Figure 9: Diagram of how the chalcopyrite surface changes during oxidation (Vaughan et al. 2002).

Figure 10: Two 2-liter Teflon reaction vessels sit inside a temperature-controlled bath. The green liquid inside the bath is antifreeze while floating Teflon balls act as insulation. Antifreeze was used instead of water to prevent corrosion of the steel baths.

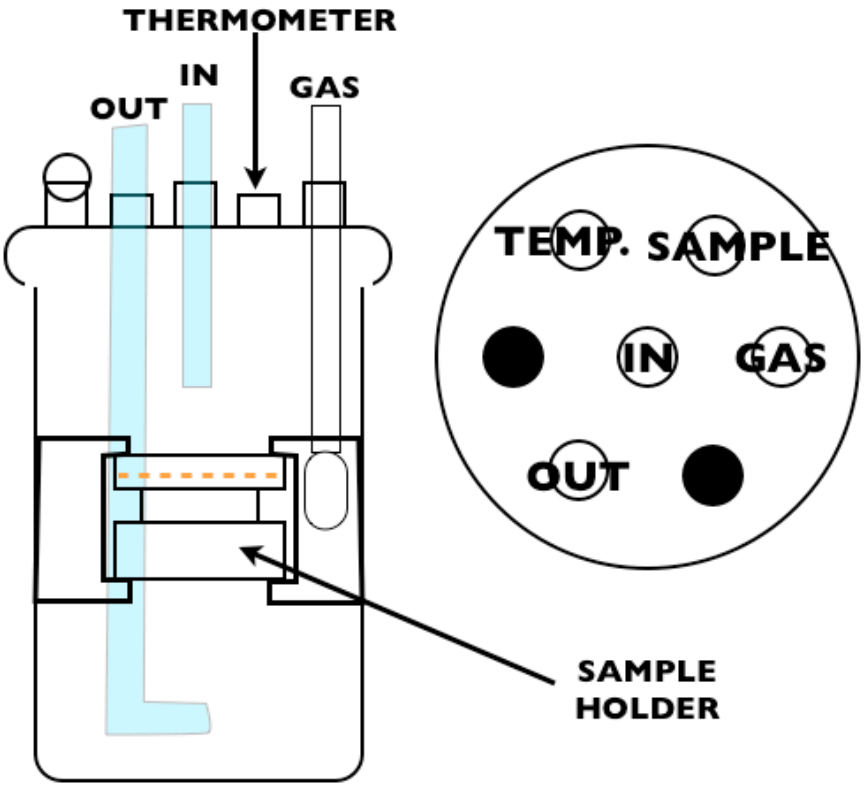

Figure 11: This cartoon cross section of the 2-liter Teflon reaction vessel illustrates the positions of tubes and ports relative to the chalcopyrite sample, based on McKibben et al., 2008. The horizontal dashed orange line denotes the approximate location of the mineral grains within the sample holder. The map view on the left side of this figure displays the container cap with built-in ports. The two black ports remained capped while the sample port was sealed between extractions by a hollow teflon ball, visible in the vessel cross section as a circle on top of the left-most port.

Figure 12: Mixing test for approximately 1L of water. In this photograph, you can see that the blue dye has dispersed homogeneously throughout the 1L beaker. Similar tests were also performed within the 2L vessels used in experiments.

Figure 13:
(A)

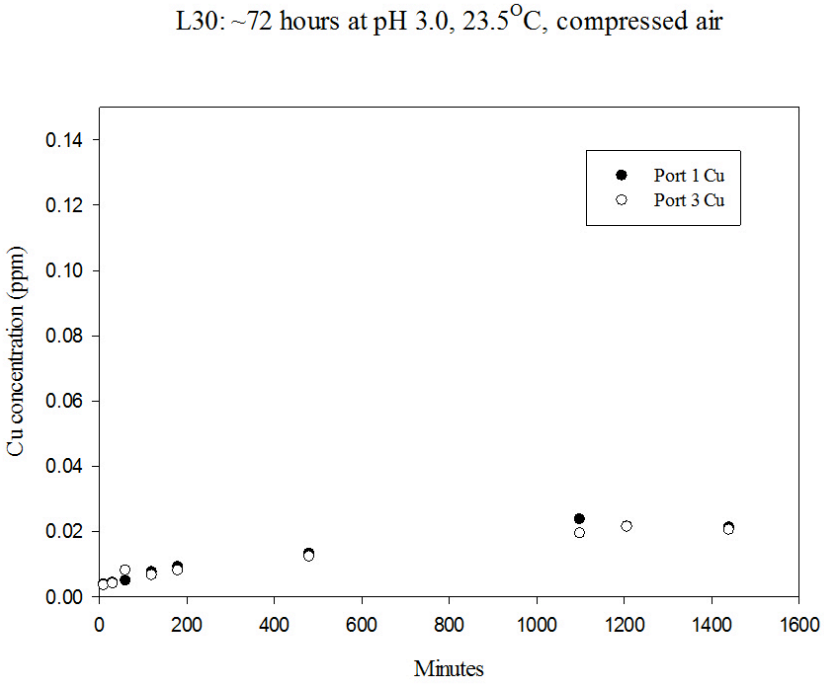

(B)

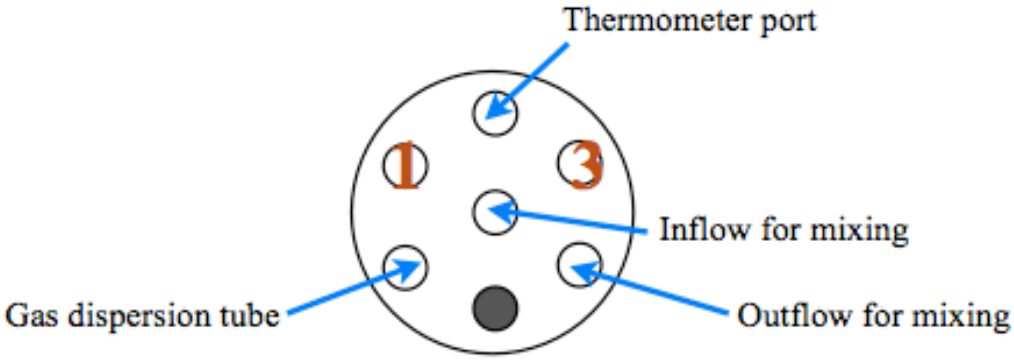

Figure 13: (A) Plot of undiluted concentrations of Cu over the course of run L30. The blue line shows data for Cu removed through Port 1 and the pink represents Cu from Port 3. By the proximity of the duplicate dots above each sample time, you can see that Cu concentrations in samples extracted from port 1 are consistent with those in samples obtained through port 3. (B) Configuration of "ports" for this experiment. The dark circle represents a closed port.

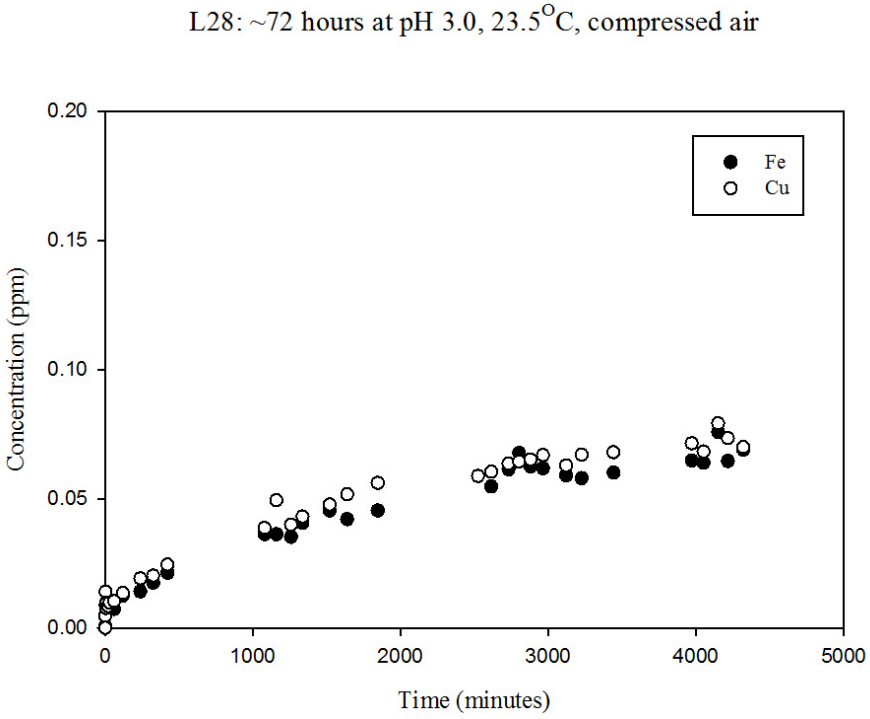

Figure 14: This is a plot of Fe and Cu concentrations in samples from experiment L28 over about 3 days.

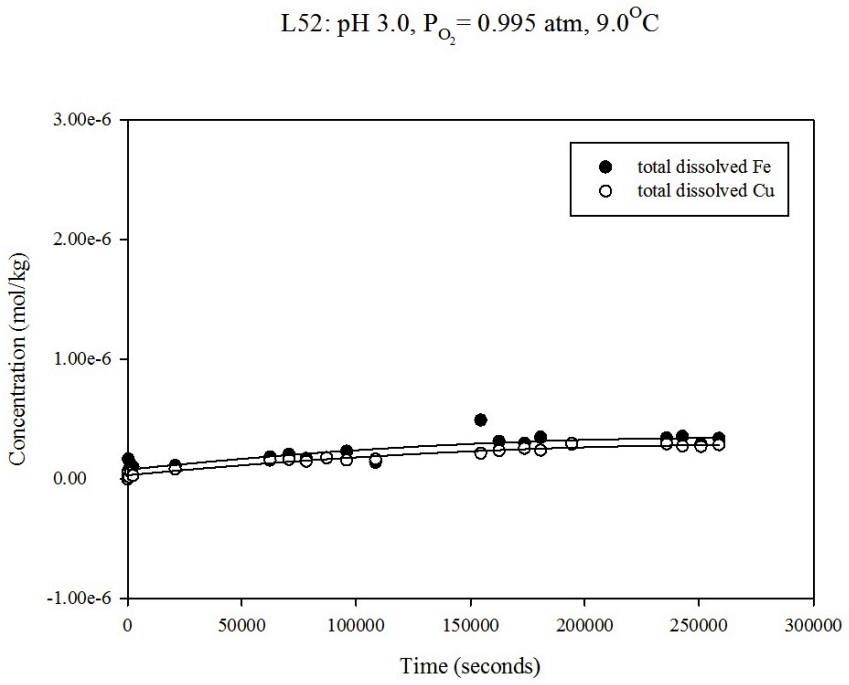

(A)

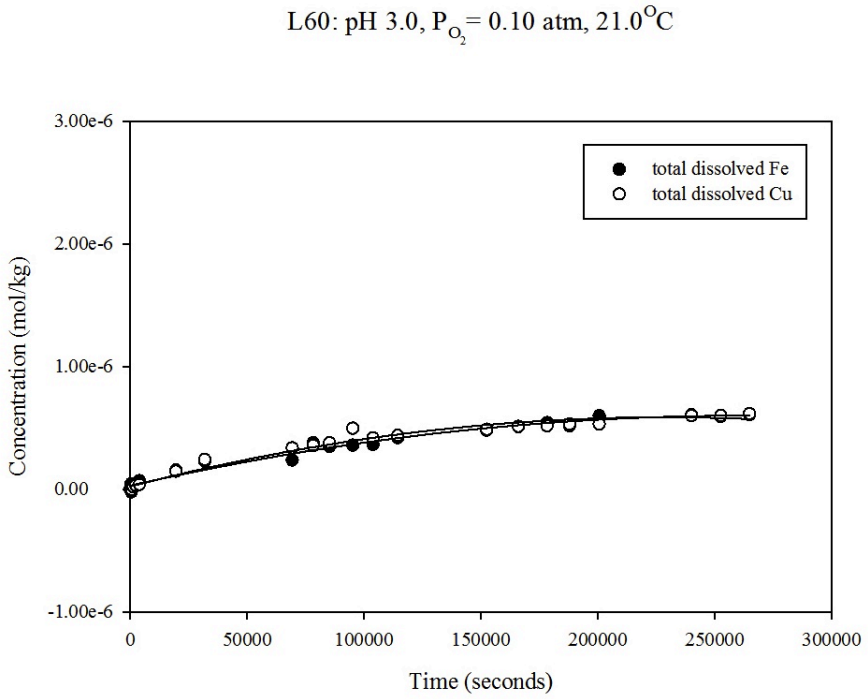

(B)

Figure 15: Under cold (A) and low P_{O2} (B) conditions, Fe and Cu appear to be released stoichiomentrically.

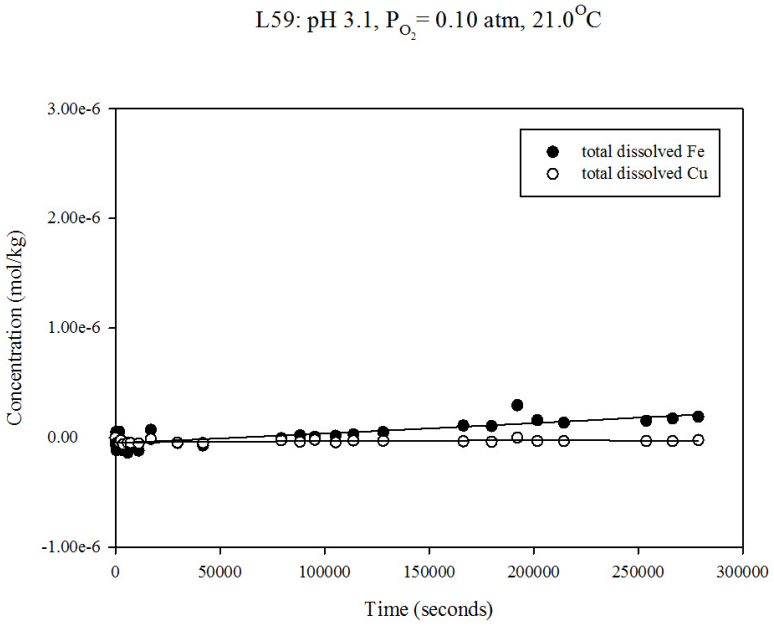

(C)

Figure 15 (continued): (C) An example of incongruent Fe and Cu data from run L59.

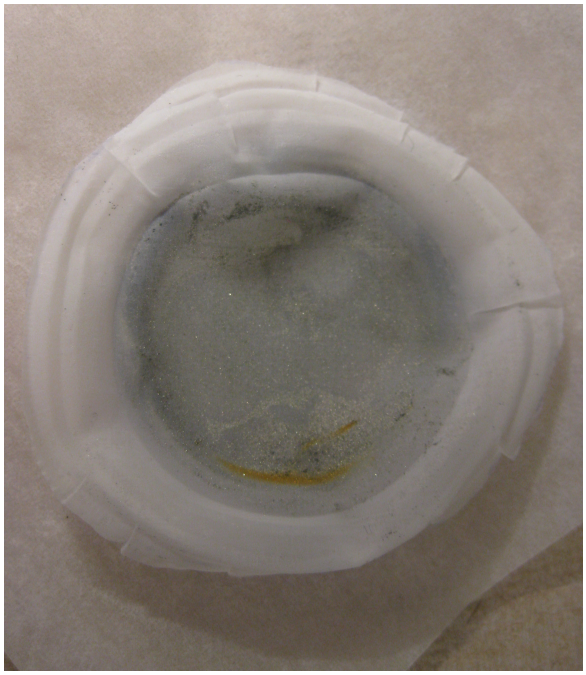

Figure 16: Post-reaction rust colored iron staining can be seen on the mesh from experiment L62, run at pH 5.2 under P_{O2} = 0.995.

(A)

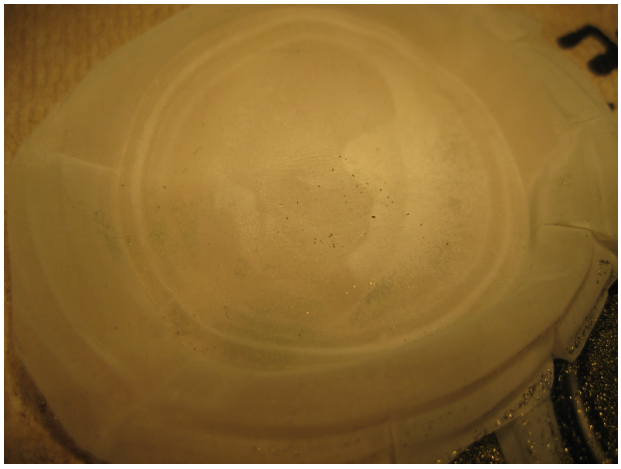

(B)

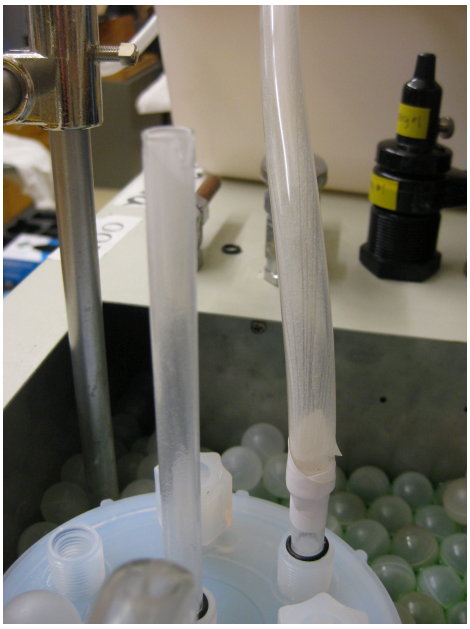

Figure 17: (A) White precipitation is visible on this top layer of mesh from experiment L74, run at pH 8.2 under P_{O2} = 0.10. (B) The same solids are seen in the tubing of experiment L73, run under identical conditions to L74.

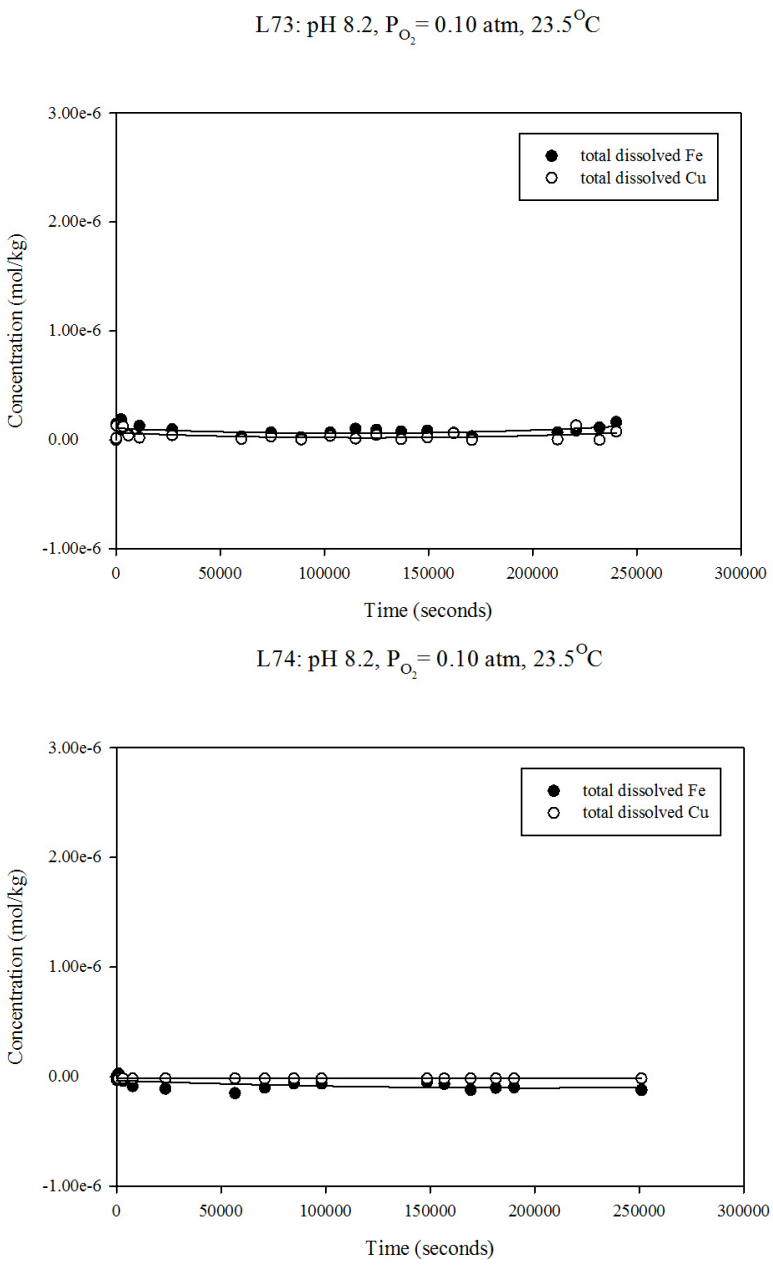

Figure 18: Reaction progression of experiments L73 and L74, run under low P_{O2} (0.10 atm) to avoid precipitates at high pH (~8.2).

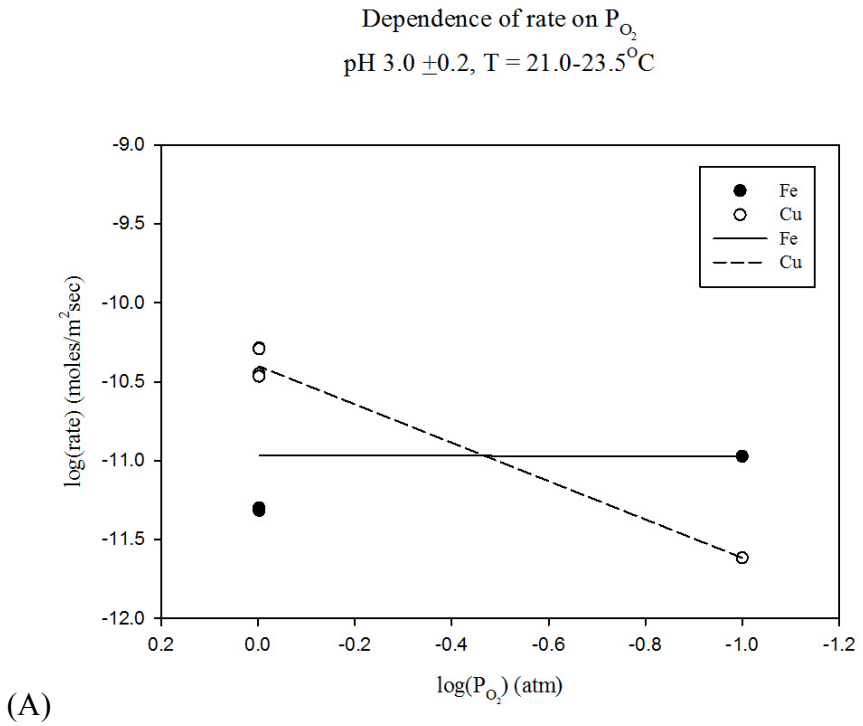

(A)

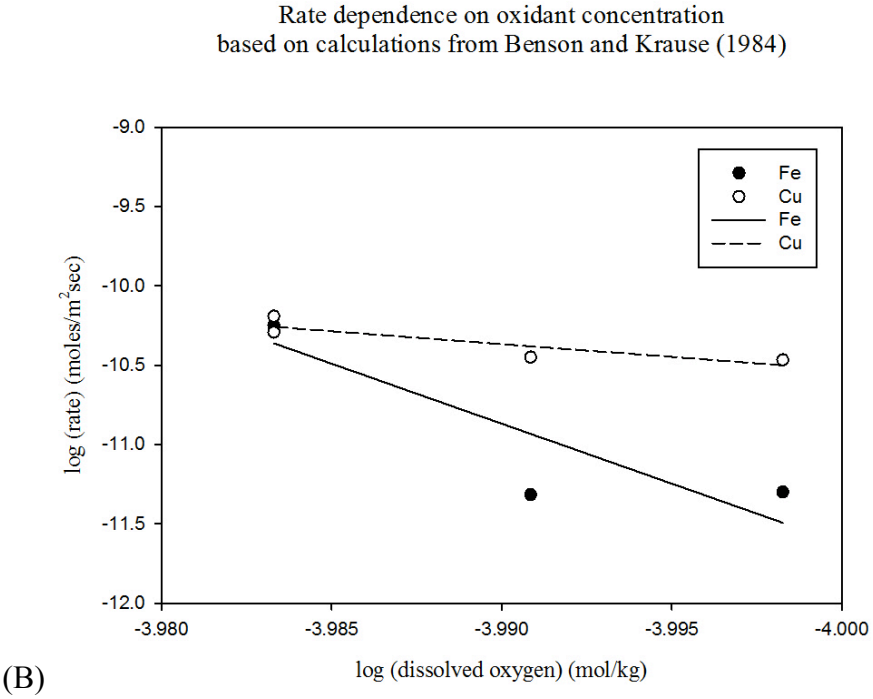

(B)

Figure 19: (A) Rate dependence on P_{O2} at pH 3.0±0.2 and room temperatures. (B) Rate dependence on dissolved O_2, estimated from calculations using values and equations from Benson and Krause (1984).

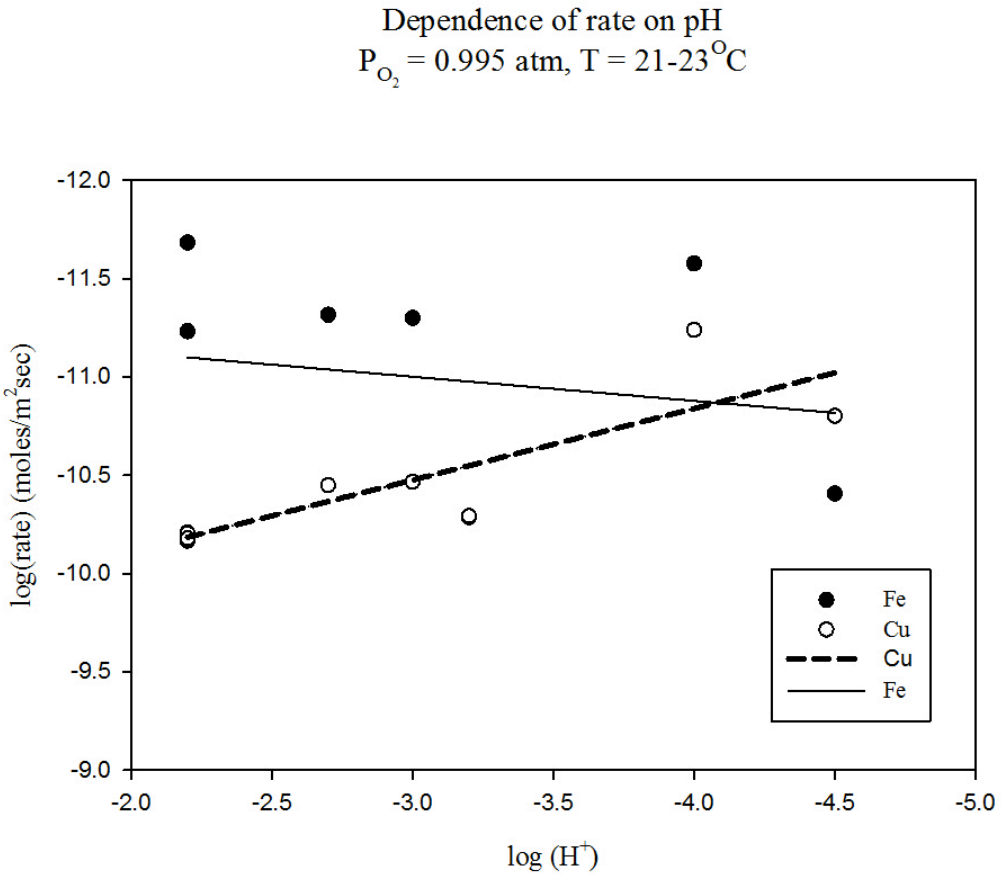

Figure 20: Rate dependence with respect to proton concentration at low pH, room temperatures, and high P_{O2}.

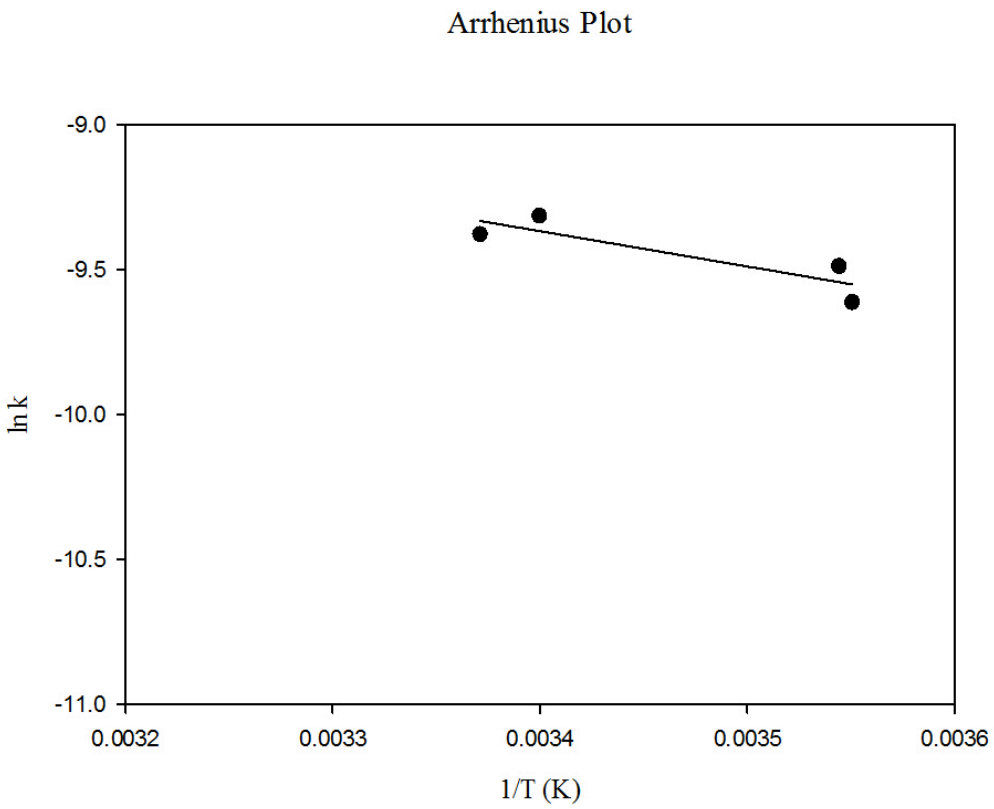

Figure 21: Arrhenius plot based on pH 3.0, P_{O_2} = 0.995 runs at 8.5, 9.0, 21.0 and 23.5°C.

Appendix A: Quantifying sample concentrations based on Inductively Coupled Mass Spectrometry (ICP-MS) data

Standard solutions of known elemental concentrations were run alongside experimental samples at the beginning and end of every ICP-MS session. Six mixtures were prepared between 0.1 ppb to 1 ppm, but the maximum concentration was later adjusted to 200 ppb to more closely bracket the sample compositions. A drift monitor, also of a known concentration, was measured repeatedly at regular intervals to track potential instrumental drift. Several techniques were attempted to obtain the most accurate data:

1. Matrix matched standards: Seawater coincident to samples compositionally and volumetrically was included in each standard along with known measurements of Cu and Fe. This mixture was diluted 10-fold with 2% trace metal grade HNO_3, as were all samples. Agilent 7500 Series ICP-MS system software converted raw data from each run to a corresponding concentration. Using this software was advantageous because it corrected for even subtle machine changes that occurred within an individual session. This is especially important for runs lasting many hours.
2. Seawater free standards: Cu and Fe were added to 2% trace metal grade HNO_3 to produce known concentrations within the range of the samples.
    a. Blank subtraction: A sample was taken from each experiment prior to interaction between the chalcopyrite and seawater. The raw counts per

second (CPS) measured by the ICP-MS in this blank was subtracted from each subsequent sample of that individual experiment to give the amount of Cu and Fe resulting from the reaction. CPS of the standards were graphed versus their expected concentrations and the equation of that line was used to convert the CPS of each sample to ppm.

b. The calculated concentration of the matrix blank was removed from samples instead of CPS to incorporate the software's compensation for machine drift, as mentioned in method 1. Negative values (caused by a more concentrated blank) were not renamed as "0" to preserve the rate. A more concentrated blank may entail precipitation during the reaction.

Matrix matching (technique 1) was not employed once it was clear that the Cu and Fe of each individual batch of seawater varied. Method 2a was also disregarded because ICP-MS sessions would often last 10 or more hours. Natural changes in analysis were likely to occur over such a long time, exacerbated by the gradual deposition of salt from synthetic seawater in the samples.

After many trials, method 2b was chosen. Although it was necessary to consider negative data in some cases, the change in the concentrations were still tracked over time. It was also preferable to utilize the software that compensates for changes in the machine throughout the analytical session.

Appendix B: Regression equations and run conditions for experiments incorporated into the rate law

Second-order polynomials were fit to graphed data in the form: $y = y_0 + ax + bx^2$. The following two tables provide the coefficients and standard error of the equations fit to Cu and Fe data for each run incorporated into the rate law. General run conditions are also included. More detailed information for individual runs can be found in Appendix C.

Nonlinear regression and condition details for Cu:

Run	y_0 (Cu)	a (initial rate Cu)	b (Cu)	Standard Error a (Cu)	T (°C)	SA (m^2)	pH	P_{O2} (atm)	A/V
L51	3.25E-08	3.30E-12	-6.58E-18	2.79E-13	9.5	0.12931	3.0	0.995	0.073141
L52	3.20E-08	1.80E-12	-3.24E-18	1.55E-13	9.0	0.12402	3.0	0.995	0.068067
L55	-1.84E-08	1.44E-12	-2.04E-18	8.06E-14	8.5	0.1287	3.0	0.995	0.07263
L59	-4.45E-08	1.87E-13	-4.62E-19	1.05E-13	21.0	0.12877	3.1	0.10	0.077528
L60	2.23E-08	4.90E-12	1.07E-17	3.11E-13	21.0	0.13307	3.0	0.10	0.076127
L67	2.27E-08	1.74E-12	-2.81E-18	1.77E-13	21.5	0.06649	3.2	0.995	0.034275
L68	8.48E-09	1.11E-12	-1.54E-18	3.55E-13	22.0	0.13057	4.5	0.995	0.070162
L69	3.39E-08	4.77E-13	-1.67E-18	3.98E-13	22.5	0.14763	4.0	0.995	0.082801
L70	-1.35E-09	-1.04E-09	3.69E-18	1.02E-12	23.0	0.13288	4.1	0.995	0.075671
L71	-1.22E-08	5.55E-12	-7.74E-18	4.41E-13	21.0	0.14692	2.2	0.995	0.083712
L73	6.41E-08	-7.47E-13	3.10E-18	3.74E-13	23.5	0.14489	8.2	0.10	0.081493
L74	-1.48E-08	-3.65E-14	1.21E-19	3.97E-14	23.5	0.1304	8.2	0.10	0.075204
L75	5.29E-08	4.60E-12	-9.14E-18	3.01E-13	22.0	0.13502	2.2	0.995	0.073619
L76	-1.65E-08	5.12E-12	-4.67E-18	3.11E-13	22.0	0.13623	2.2	0.995	0.075184
L77	2.70E-07	2.87E-12	-1.73E-18	2.73E-13	23.0	0.14379	2.7	0.995	0.080827
L78	2.37E-08	2.68E-12	-4.21E-18	1.84E-13	23.5	0.13551	3.0	0.995	0.078422

Nonlinear regression and condition details for Fe:

Run	y_0 (Fe)	a (initial rate Fe)	b (Fe)	Standard Error a (Fe)	T (°C)	SA (m^2)	pH	P_{O2} (atm)	A/V
L51	6.83E-08	1.93E-12	-2.34E-18	7.53E-13	9.5	0.129313	3.0	0.995	0.073141
L52	7.77E-08	1.99E-12	-3.78E-18	5.16E-13	9.0	0.124019	3.0	0.995	0.068067
L55	1.01E-07	1.81E-12	-3.38E-18	4.98E-13	8.5	0.1287	3.0	0.995	0.07263
L59	-4.85E-08	8.24E-13	3.76E-19	4.33E-13	21.0	0.128774	3.1	0.10	0.077528
L60	2.89E-08	4.29E-12	-8.13E-18	2.58E-13	21.0	0.133071	3.0	0.10	0.076127
L67	5.33E-08	1.77E-12	-2.75E-18	4.42E-13	21.5	0.066493	3.2	0.995	0.034275
L68	-1.33E-08	2.75E-12	-1.15E-18	6.68E-13	22.0	0.130572	4.5	0.995	0.070162
L69	1.03E-07	2.65E-12	-2.68E-18	8.46E-13	22.5	0.147634	4.0	0.995	0.082801
L70	-2.51E-07	2.83E-12	-3.53E-18	7.29E-13	23.0	0.132878	4.1	0.995	0.075671
L71	-4.25E-08	5.18E-12	-6.10E-18	6.12E-13	21.0	0.146915	2.2	0.995	0.083712
L73	1.06E-07	-8.45E-13	3.79E-18	3.77E-13	23.5	0.144894	8.2	0.10	0.081493
L74	-3.43E-08	-6.77E-13	1.69E-18	3.86E-13	23.5	0.130405	8.2	0.10	0.075204
L75	3.19E-08	2.07E-12	-3.23E-18	9.93E-13	22.0	0.135017	2.2	0.995	0.073619
L76	2.10E-07	5.86E-12	-8.21E-18	8.25E-13	22.0	0.136233	2.2	0.995	0.075184
L77	1.68E-07	4.83E-12	-1.10E-17	8.69E-13	23.0	0.14379	2.7	0.995	0.080827
L78	1.01E-07	5.01E-12	-1.10E-17	7.70E-13	23.5	0.135513	3.0	0.995	0.078422

Appendix C: ICP-MS data and run details from all experiments under compressed air or oxygen mixtures

Please note: All temperatures (T) are provided in °C and each experimental sample extracted was 1 mL unless described otherwise. Any missing samples were not used to derive the rate (i.e. due to soap contamination, etc.). Cu and Fe molar concentrations were calculated as described in Appendix A.

L51: 9.5°C, P_{O2} = 0.995 atm, pH = 3.0

Time passed (minutes)	Label	Dilution factor (by mass)	T (bath)	T (vessel)	Cu (Molar)	Fe (Molar)	Notes
0	L51-0	10.88	N/A	~5	0.00E+00	0.00E+00	blank during T equilibration, vessel purge 4:20-4:30 PM
2	L51-1	10.22	~8	8.2	9.28E-07	8.25E-08	contact @ 4:31:45 PM, BUBBLES DOWN after L51-1
5	L51-2	10.69	~8	8.2	9.40E-07	-9.37E-08	
10	L51-3	10.55	~8	9.2	1.14E-06	3.39E-08	
19	L51-4	10.65	6.0	10	1.30E-06	3.47E-07	
33	L51-5	10.70	6.0	10.7	1.21E-06	1.87E-07	bath T set DOWN
60	L51-6	10.69	4.0	11.1	7.05E-07	1.59E-08	O off @ 5:44 for split with L52
116	L51-7	10.77	3.8	9.9	6.64E-07	3.08E-08	EXTRA SAMPLE TAKEN AND DISCARDED
424	L51-8	10.53	3.0	9.8	4.11E-07	1.23E-07	BUBBLES OFF for a couple of minutes: line kicked.
1116	L51-9	10.26	3.5	9.6	2.07E-07	1.58E-07	
1241	L51-10	10.93	3.5	9.6	4.48E-07	1.99E-07	
1367	L51-11	10.84	3.5	9.8	3.37E-07	2.10E-07	
1516	L51-12	10.70	3.5	9.3	2.19E-07	1.94E-07	
1663	L51-13	10.85	3.5	9.2	2.01E-07	1.95E-07	
2504	L51-15	10.65	3.5	9.4	-4.30E-07	2.29E-07	
2698	L51-16	10.65	3.5	9.6	-4.81E-08	4.79E-07	
2833	L51-17	10.75	3.5	9.6	3.82E-08	3.31E-07	
3039	L51-18	10.96	4.0	9.9	1.52E-07	3.60E-07	
4075	L51-21	10.82	3.8	9.6	-1.36E-07	3.66E-07	
4200	L51-22	10.72	3.5	9.6	-2.37E-07	3.83E-07	
4335	L51-23	10.82	3.5	9.6	-3.14E-08	4.81E-07	
4468	L51-24	10.70	3.5	9.7	-2.68E-07	3.67E-07	

L52: 9.0°C, P_{O2} = 0.995 atm, pH = 3.0

Time passed (minutes)	Label	Dilution factor (by mass)	T (bath)	T (vessel)	Cu (Molar)	Fe (Molar)	Notes
0	L52-0	10.59	4.6	~8	0.00E+00	0.00E+00	blank during T equilibration
3	L52-1	10.61	4.0	<10	2.29E-08	6.11E-08	fill @ 5:52 PM, O @ 5:53:40 PM
5	L52-2	10.63	4.0	9.0	5.36E-08	1.66E-07	
11	L52-3	10.56	4.0	9.0	1.87E-08	7.81E-08	
22	L52-4	10.59	4.0	9.0	5.62E-08	1.22E-07	
39	L52-5	10.60	3.8	8.9	2.92E-08	1.01E-07	
347	L52-6	10.46	3.0	9.0	8.18E-08	1.10E-07	BUBBLES OFF for a couple of minutes: line kicked.
1039	L52-7	10.56	3.5	9.0	1.56E-07	1.83E-07	
1176	L52-8	10.80	3.5	9.0	1.62E-07	2.05E-07	
1302	L52-9	10.55	3.5	9.0	1.47E-07	1.71E-07	
1451	L52-10	10.73	3.5	9.0	1.75E-07	1.77E-07	
1598	L52-11	10.52	3.5	9.0	1.57E-07	2.29E-07	
1808	L52-12	10.37	3.0	9.0	1.64E-07	1.39E-07	TUBING SHIFTED @ 11:48-49 PM
2439	L52-13	10.50	3.5	9.0			not used due to soap contamination
2574	L52-14	10.48	3.5	9.0	2.13E-07	4.88E-07	
2708	L52-15	10.60	3.5	9.0	2.37E-07	3.12E-07	
2893	L52-16	10.69	4.0	9.5	2.55E-07	2.95E-07	
3011	L52-17	10.51	4.0	9.9	2.39E-07	3.47E-07	
3239	L52-18	11.06	3.5	8.5	2.94E-07	2.88E-07	
3929	L52-19	10.60	3.8	9.0	2.90E-07	3.39E-07	
4045	L52-20	10.63	3.5	9.0	2.72E-07	3.52E-07	
4180	L52-21	10.68	3.5	8.5	2.69E-07	2.89E-07	
4312	L52-22	10.49	3.5	8.0	2.84E-07	3.37E-07	

L55: 8.5°C, P_{O_2} = 0.995 atm, pH = 3.0

Time passed (minutes)	Label	Dilution factor (by mass)	T (bath)	T (vessel)	Cu (Molar)	Fe (Molar)	Notes
0	L55-0	7.228	N/A	6.9	0.00E+00	0.00E+00	blank during T-equilibration (not purged with O2)
2	L55-1	10.506	4	~8	-2.33E-08	3.21E-08	fill @ 12:54:52 PM, O2 before (because vessel was purged)
3	L55-2	10.351	4	8.1	-1.14E-08	1.01E-07	
6.5	L55-3	10.675	4	8.1	-2.06E-08	9.84E-08	
10	L55-4	10.538	4	8.3			
20	L55-5	10.642	4	8.5			
30	L55-6	10.560	4	8.6	-2.04E-08	6.57E-08	
62	L55-7	18.912	4	9	4.04E-09	3.30E-07	
104	L55-8	10.375	4	8.8	-1.21E-08	1.05E-07	
159	L55-9	10.454	3.5	8.5	-1.68E-08	1.16E-07	3:41-42: O2 split to share with L56
220	L55-10	10.527	3.7	8.4	-1.19E-08	1.18E-07	
280	L55-11	10.372	4	8.2	4.77E-09	1.25E-07	
411	L55-12	10.476	3.5	8.1	6.89E-09	1.41E-07	
613	L55-13	10.610	3.5	8	2.90E-08	1.68E-07	
1107	L55-14	10.634	3.5	8	6.64E-08	1.96E-07	
1285	L55-15	10.495	3.5	8.8			O2 OFF (L56 FAIL!!!) + tubing shift after sample @ 10:23 AM
1396	L55-16	10.689	4	8.4	8.86E-08	2.33E-07	
1500	L55-17	10.856	3.8	7.4	1.02E-07	2.52E-07	
1706	L55-18	10.400	3.2	7.2	1.20E-07	2.75E-07	soapy sample, not included in rate
1894	L55-19	10.751	3	7.2			soapy sample, not included in rate
2060	L55-20	10.605	3	7	1.30E-07	2.91E-07	TUBING SHIFTED AFTER L55-20
2673	L55-21	10.433	3.3	7.3	1.68E-07	2.68E-07	
2803	L55-22	10.501	3	7.3	1.62E-07	2.94E-07	
2961	L55-23	10.613	3	7.4	1.59E-07	3.00E-07	
3109	L55-24	10.445	3	7.3			TUBING SHIFTED AFTER L55-24
3312	L55-25	10.360	3	7.2			
3511	L55-26	10.564	3	7.2			soapy sample, not included in rate
4085	L55-27	10.467	3.2	7.2			soapy sample, not included in rate
4215	L55-28	10.294	3.2	7.2	2.29E-07	3.54E-07	
4420	L55-29	10.180	3	7.2	2.14E-07	3.51E-07	

L59: 21.0°C, P_{O_2} = 0.10 atm, pH = 3.1

Time passed (minutes)	Label	Dilution factor (by mass)	T (bath)	T (vessel)	Cu (Molar)	Fe (Molar)	Notes
0	L59-0	11.00	N/A	N/A	0.00E+00	0.00E+00	blank during purge
3	L59-1	10.63	21.0	~20	-5.93E-08	3.21E-08	GAS @ 11:07 AM, FILL @ 11:09:53 AM
5	L59-2	10.73	21.0	~20	-5.43E-08	1.01E-07	bubbles on again
9	L59-3	10.72	20.0	~20	-6.24E-08	9.84E-08	
15	L59-4	10.70	20.0	19.9	-5.48E-08	6.57E-08	
21	L59-5	10.67	20.0	20.0	-4.41E-08	3.30E-07	
30	L59-6	10.47	20.0	20.6	-3.99E-08	1.05E-07	
44	L59-7	10.78	20.0	21.0	-2.31E-08	1.16E-07	
60	L59-8	10.53	20.0	21.1	-5.92E-08	1.18E-07	
98	L59-9	10.30	20.0	21.8	-4.71E-08	1.25E-07	
120	L59-10	10.48	20.0	21.6	-4.91E-08	1.41E-07	GAS SPLIT FOR L60 @ 1:12 PM
185	L59-11	10.01	20.0	21.4	-5.29E-08	1.68E-07	2:11 (BEFORE SAMPLE): bubbles about even (splitting problems...)
282	L59-12	10.58	19.7	21.2	-1.21E-08	1.96E-07	
494	L59-13	10.47	19.0	21.0	-4.51E-08	2.33E-07	
698	L59-14	10.27	19.2	21.0	-4.89E-08	2.52E-07	
1321	L59-15	10.13	19.0	21.0	-2.34E-08	2.75E-07	
1471	L59-16	10.33	19.0	21.2	-3.62E-08	2.91E-07	
1588	L59-17	10.49	19.0	21.0	-1.87E-08	2.68E-07	
1754	L59-18	10.40	19.0	21.0	-4.11E-08	2.94E-07	
1897	L59-19	10.42	19.0	21.2	-2.56E-08	3.00E-07	GAS OFF!!
2134	L59-20	10.33	19.0	21.0	-2.78E-08	3.54E-07	
2772	L59-21	10.49	19.0	21.0	-3.32E-08	3.51E-07	
2998	L59-22	10.35	19.0	21.2	-3.65E-08	0.00E+00	2:09 PM: TUBING SHIFT
3203	L59-23	10.57	19.0	21.5	2.21E-10	3.21E-08	
3362	L59-24	10.60	19.2	22.0	-2.98E-08	1.01E-07	
3574	L59-25	10.50	19.2	21.0	-3.11E-08	9.84E-08	
4230	L59-26	10.35	19.2	21.0	-2.96E-08	6.57E-08	
4440	L59-27	10.54	19.0	21.6	-3.25E-08	3.30E-07	
4645	L59-28	10.42	19.0	21.2	-2.13E-08	1.05E-07	

L60: 21.0°C, P_{O_2} = 0.10 atm, pH = 3.0

Time passed (minutes)	Label	Dilution factor (by mass)	T (bath)	T (vessel)	Cu (Molar)	Fe (Molar)	Notes
0	L60-0	10.76	N/A	N/A	0.00E+00	0.00E+00	blank during purge
3	L60-1	10.68	20.0	~20			GAS @ 1:55 PM, fill @ 1:57:36PM
5.5	L60-2	10.53	20.0	~20	2.91E-09	4.10E-08	GAS SPLITTING PROBLEMS: very vigorous bubbles so both vessels receive the gas mixtures
8	L60-3	10.48	20.0	~20	-1.16E-08	-2.20E-08	
10	L60-4	10.35	20.0	20.0	-2.69E-09	3.84E-09	2:11PM: BUBBLES EVEN (used hose clamp)
22	L60-5	10.48	20.0	20.0	1.74E-08	2.59E-08	
40	L60-6	10.32	20.0	19.7	3.08E-08	4.64E-08	
65	L60-7	10.35	21.0	19.5	3.77E-08	6.74E-08	
115	L60-8	10.60	21.0	19.7			
326	L60-9	10.52	19.0	21.0	1.46E-07	1.54E-07	
531	L60-10	10.51	19.0	20.9	2.40E-07	2.26E-07	
1154	L60-11	10.31	19.2	21.0	3.33E-07	2.35E-07	
1304	L60-12	10.63	19.0	21.0	3.54E-07	3.74E-07	
1421	L60-13	10.60	19.0	21.0	3.73E-07	3.46E-07	
1586	L60-14	10.58	19.0	21.0	4.93E-07	3.55E-07	
1730	L60-15	10.39	19.0	21.0	4.14E-07	3.62E-07	7:44PM: GAS OFF!! pressure of tank dropped, nozzle not open enough.
1906	L60-16	10.33	19.0	21.0	4.33E-07	4.17E-07	
2540	L60-17	10.46	19.0	21.0	4.84E-07	4.77E-07	
2766	L60-18	10.49	19.0	21.2	5.07E-07	5.06E-07	2:09PM: TUBING SHIFT
2971	L60-19	10.42	19.0	21.7	5.12E-07	5.36E-07	
3130	L60-20	10.45	19.2	22.0	5.25E-07	5.13E-07	
3342	L60-21	10.38	19.2	21.0	5.26E-07	5.92E-07	
3999	L60-22	10.42	19.2	21.2	5.95E-07	6.00E-07	
4208	L60-23	10.42	19.0	21.6	5.95E-07	5.88E-07	
4413	L60-24	10.41	19.0	21.2	6.11E-07	6.03E-07	DONE

L67: 21.5°C, P_{O_2} = 0.995 atm, pH = 3.2

Time passed (minutes)	Label	Dilution factor (by mass)	T (bath)	T (vessel)	Cu (Molar)	Fe (Molar)	Notes
0	L67-0	10.69	N/A	N/A	0.00E+00	0.00E+00	blank during purge
3	L67-1	10.42	19.5	~20	1.16E-08	3.93E-08	fill @ 11:58:50 AM, O2 @ 12:01 PM
6	L67-2	10.38	19.5	~20	-2.00E-09	4.28E-08	
10	L67-3	11.00	19.5	~20.5	3.07E-08	4.35E-08	
20	L67-4	10.64	19.5	20.6	1.24E-08	7.94E-08	O2 SPLIT: FOR L68
34	L67-5	10.77	19.5	21.1	6.94E-08	8.55E-08	
65	L67-6	10.76	19.5	21.4	3.49E-08	1.86E-07	
98	L67-7	10.67	19.5	21.4	5.19E-08	5.58E-08	
140	L67-8	10.72	19.5	21.5	2.69E-08	4.37E-08	BUBBLES UP
200	L67-9	10.24	19.7	21.5	4.12E-08	7.61E-08	
322	L67-10	10.64	19.5	21.3	5.58E-08	7.13E-08	
474	L67-11	9.64	19.5	21.3	6.85E-08	8.53E-08	
696	L67-12	10.64	19.2	21.0	9.36E-08	1.33E-07	
1337	L67-13	10.69	19.9	21.5	1.92E-07	2.02E-07	
1476	L67-14	10.41	20.0	21.5			
1594	L67-15	10.47	19.5	21.4	1.54E-07	1.48E-07	
1768	L67-16	10.63	19.5	21.5	1.58E-07	1.63E-07	
1923	L67-17	10.74	19.5	22.2	1.95E-07	1.97E-07	
2092	L67-18	10.50	19.5	21.2	1.93E-07	1.76E-07	
2748	L67-19	10.60	20.0	21.3	2.15E-07	3.38E-07	
2887	L67-20	10.72	19.9	21.4	2.14E-07	2.54E-07	
3081	L67-21	10.58	19.7	21.4			3:38 PM: tubing shift
3324	L67-22	10.63	19.5	21.4	2.46E-07	3.08E-07	
3527	L67-23	10.78	20.0	21.1	3.05E-07	4.48E-07	
4188	L67-24	10.44	20.0	21.3	2.91E-07	3.77E-07	DOUBLE SAMPLE
4314	L67-25	10.76	20.0	21.6	3.15E-07	3.24E-07	
4476	L67-26	10.41	20.0	21.8	2.54E-07	2.18E-07	

L68: 22.0°C, P_{O_2} = 0.995 atm, pH = 4.5

Time passed (minutes)	Label	Dilution factor (by mass)	T (bath)	T (vessel)	Cu (Molar)	Fe (Molar)	Notes
0	L68-0	10.75	N/A	N/A	0.00E+00	0.00E+00	blank during purge
3	L68-1	10.58	19.5	~20.3	8.58E-09	-9.67E-09	fill @ 1:06:07 PM, O2 @ 1:07 PM
5.5	L68-2	10.58	19.5	20.4	1.54E-08	-3.54E-08	
10	L68-3	10.41	19.5	20.6	1.75E-08	-4.82E-08	Sample taken a little shallow??
20	L68-4	10.67	19.5	20.9	2.22E-08	1.30E-08	
46	L68-5	10.40	19.5	21.5	1.60E-08	-1.48E-08	
71	L68-6	10.62	19.5	21.7	1.23E-08	1.51E-09	
133	L68-7	10.48	19.7	22.0	4.46E-08	1.72E-07	
254	L68-8	10.42	19.5	22.0	1.98E-08	1.89E-08	
407	L68-9	10.05	19.2	21.8	1.49E-08	7.94E-09	
629	L68-10	10.50	19.9	21.7	5.36E-08	1.44E-07	
1270	L68-11	10.59	20.0	21.9	4.76E-08	1.12E-07	
1408	L68-12	10.34	19.5	22.0	1.36E-07	1.39E-07	
1527	L68-13	10.50	19.5	22.0	9.50E-08	1.56E-07	
1701	L68-14	10.51	19.5	22.2	5.75E-08	1.80E-07	
1855	L68-15	10.50	19.5	22.1	7.12E-08	2.19E-07	
2025	L68-16	10.45	19.5	21.8	7.17E-08	2.25E-07	
2681	L68-17	10.31	20.0	22.0	1.79E-07	5.27E-07	
2820	L68-18	10.59	19.9	22.0	1.12E-07	5.24E-07	
3013	L68-19	10.52	19.7	22.0	2.42E-07	5.91E-07	
3262	L68-20	10.33	19.5	21.8			TUBING SHIFT: 3:38 PM
3460	L68-21	10.63	20.0	21.7	2.85E-07	5.89E-07	
4122	L68-22	10.31	20.0	21.8	1.52E-07	5.22E-07	
4248	L68-23	10.48	20.0	22.0	1.37E-07	5.22E-07	
4411	L68-24	10.22	20.0	22.1			

L69: 22.5°C, P_{O_2} = 0.995 atm, pH = 4.0

Time passed (minutes)	Label	Dilution factor (by mass)	T (bath)	T (vessel)	Cu (Molar)	Fe (Molar)	Notes
0	L69-0	10.51	N/A	N/A	0.00E+00	0.00E+00	blank during fill
3.5	L69-1	10.70	22.0	~19	3.81E-08	8.43E-08	fill @ 6:21:06 PM, O2 @ 6:23:46 PM (after fill)
5	L69-2	10.60	22.0	~19	3.53E-08	1.44E-07	
10	L69-3	10.68	22.0	20.0	1.78E-08	4.01E-08	
20	L69-4	10.69	22.0	21.0	2.60E-08	6.67E-08	6:32 PM: O2 SPLIT FOR L70
36	L69-5	10.65	22.0	21.5	5.41E-08	3.88E-07	
64	L69-6	10.51	22.0	22.0	1.94E-08	3.92E-08	
98	L69-7	10.47	22.0	22.5	3.59E-08	5.29E-08	
315	L69-8	10.37	22.0	22.2	6.94E-08	1.68E-07	
956	L69-9	10.43	22.0	23.0	7.22E-08	1.65E-07	
1094	L69-10	10.38	22.0	22.9	4.96E-08	3.88E-07	
1213	L69-11	10.55	22.0	23.0	4.01E-08	2.33E-07	
1387	L69-12	10.50	22.0	22.5	6.81E-08	3.89E-07	
1542	L69-13	10.46	22.0	22.2	5.02E-08	2.77E-07	
1716	L69-14	10.52	22.0	22.5	2.33E-07	4.72E-07	
2366	L69-15	10.31	22.0	22.5	3.31E-08	3.83E-07	
2506	L69-16	10.61	22.0	22.9	3.17E-08	4.37E-07	
2699	L69-17	10.47	22.0	22.5	2.57E-08	4.57E-07	
2948	L69-18	10.32	22.0	22.5	3.02E-08	3.74E-07	3:40 PM: TUBING SHIFT
3145	L69-19	10.43	22.0	22.2	3.59E-08	4.19E-07	
3809	L69-20	10.42	22.0	22.2	2.21E-08	7.55E-07	
3934	L69-21	10.43	22.0	22.6	1.54E-07	6.32E-07	
4098	L69-22	10.22	22.0	23.0	1.96E-08	4.73E-07	
4215	L69-23	10.66	22.0	22.5	6.66E-08	6.18E-07	

L70: 23.0°C, P_{O2} = 0.995 atm, pH = 4.1

Time passed (minutes)	Label	Dilution factor (by mass)	T (bath)	T (vessel)	Cu (Molar)	Fe (Molar)	Notes
0	L70-0	10.56	N/A	N/A	0.00E+00	0.00E+00	blank during FILL
1	L70-1	10.39	22.0	~19	4.73E-07	-3.74E-07	fill @ 7:20:36 PM, O2 @ 7:22:30 (after fill)
4.5	L70-2	10.45	22.0	~19	-9.26E-08	-2.34E-07	
10	L70-3	10.43	22.0	20.0	-6.46E-08	-3.04E-07	
19	L70-4	10.48	22.0	21.0	-1.02E-07	-3.48E-07	
40	L70-5	10.48	22.0	22.0	-5.26E-08	-2.47E-07	
95	L70-6	10.30	22.0	23.0	-9.83E-08	-2.86E-07	
197	L70-7	10.26	22.0	23.0	-8.90E-08	-2.35E-07	
839	L70-8	10.45	22.0	23.0	-6.70E-08	-5.45E-08	
976	L70-9	10.57	22.0	23.0	-7.04E-08	-4.60E-08	
1095	L70-10	10.35	22.0	23.0	-7.22E-08	-8.26E-08	
1269	L70-11	10.28	22.0	23.0	-6.52E-08	-9.28E-08	
1424	L70-12	10.32	22.0	23.0	-2.89E-08	6.18E-08	
1592	L70-13	10.27	22.0	23.0	-7.26E-08	1.14E-09	
2249	L70-14	10.26	22.0	23.0	-6.90E-08	2.40E-08	
2388	L70-15	10.48	22.0	23.0	-5.47E-08	7.41E-08	
2581	L70-16	10.40	22.0	23.0	-6.36E-08	7.89E-08	
2830	L70-17	10.15	22.0	23.2	-6.66E-08	2.02E-08	3:42 PM: TUBING SHIFT
3027	L70-18	10.43	22.0	23.0	-5.16E-08	1.89E-07	
3690	L70-19	10.32	22.0	23.0	-3.26E-08	2.17E-07	
3815	L70-20	10.29	22.0	23.0	5.27E-08	1.32E-06	
3981	L70-21	10.28	22.0	23.0	-5.86E-08	1.74E-07	
4097	L70-22	10.49	22.0	23.0	-4.83E-08	3.08E-07	

L71: 21.0°C, P_{O_2} = 0.995 atm, pH = 2.2

Time passed (minutes)	Label	Dilution factor (by mass)	T (bath)	T (vessel)	Cu (Molar)	Fe (Molar)	Notes
0	L71-0	10.51	N/A	N/A	0.00E+00	0.00E+00	blank during purge
3	L71-1	10.30	~19	~20	-4.49E-08	-1.22E-07	fill @ 3:35:40 PM, O2 @ 3:38PM
6	L71-2	10.59	19.5	20.0	-6.73E-08	-6.30E-08	
9	L71-3	10.54	19.5	20.0	-2.89E-08	7.16E-10	
20	L71-4	10.57	19.5	20.0	-5.10E-08	-1.30E-07	O2 SPLIT FOR L72 after this sample
34	L71-5	10.69	19.5	20.7	8.31E-06	7.31E-08	
60	L71-6	10.66	19.5	21.0	1.14E-07	9.84E-09	
80	L71-7	10.62	19.5	21.0	-2.95E-08	-3.48E-08	
119	L71-8	10.53	19.5	21.0	1.49E-07	9.05E-08	
257	L71-9	10.42	19.3	21.0	4.62E-08	6.83E-08	
464	L71-10	10.54	19.9	21.0	9.86E-08	4.94E-08	
1098	L71-11	10.47	19.9	21.0	2.82E-07	1.47E-07	
1271	L71-12	10.61	19.4	21.0	3.55E-07	2.34E-07	
1482	L71-13	10.54	19.3	21.0	5.28E-07	3.55E-07	
1575	L71-14	10.65	19.5	21.0	4.81E-07	3.69E-07	
1838	L71-15	10.60	19.3	20.8	4.85E-07	5.13E-07	
2392	L71-16	10.55	19.5	20.8	5.93E-07	5.36E-07	
2628	L71-17	10.62	19.5	21.0	6.81E-07	7.82E-07	
2871	L71-18	10.57	19.5	21.0	6.94E-07	6.40E-07	
3101	L71-19	10.45	19.5	21.0	7.20E-07	8.18E-07	
3305	L71-20	10.44	19.5	21.0	7.53E-07	6.83E-07	7:20 PM: TUBING SHIFT
3951	L71-21	10.66	19.5	21.0	8.91E-07	8.68E-07	
4083	L71-22	10.54	19.5	21.0	9.17E-07	8.75E-07	
4319	L71-23	10.37	19.5	21.0	8.92E-07	8.12E-07	

L73: 23.5°C, P_{O_2} = 0.10 atm, pH = 8.2

Time passed (minutes)	Label	Dilution factor (by mass)	T (bath)	T (vessel)	Cu (Molar)	Fe (Molar)	Notes
0	L73-0	10.69	N/A	N/A	0.00E+00	0.00E+00	blank during fill
1.5	L73-1	10.66	~20	~20	1.50E-08	1.44E-07	fill @ 2:35:13 PM, gas @ 2:32 PM (vessel purged BEFORE fill!!)
5.5	L73-2	10.67	~18	19.7	1.30E-07	1.38E-07	BATH ON NOW!
10	L73-3	10.56	19.0	19.7			
20	L73-4	10.66	20.8	20.0			GAS SPLIT @ 2:48PM FOR L74
41	L73-5	10.69	22.0	22.2	1.14E-07	1.86E-07	
57	L73-6	10.62	22.0	22.9	1.22E-07	8.85E-08	GAS TEMPORARILY OFF FOR L74 VESSEL PURGE
99	L73-7	10.51	22.0	23.1	4.06E-08	4.95E-08	
187	L73-8	10.44	22.0	23.2	2.01E-08	1.26E-07	
450	L73-9	10.44	22.0	23.4	4.29E-08	9.54E-08	
1004	L73-10	10.22	22.0	23.5	8.51E-09	3.00E-08	
1241	L73-11	10.55	22.0	23.7	3.07E-08	6.76E-08	
1482	L73-12	10.46	22.0	23.7	2.89E-09	2.29E-08	
1713	L73-13	10.44	22.0	23.6	3.55E-08	6.59E-08	WHITE PRECIPITATE SEEN! (possibly earlier)
1917	L73-14	10.41	22.0	23.4	1.15E-08	1.01E-07	
2083	L73-15	10.21	22.0	23.4	4.63E-08	9.18E-08	
2281	L73-16	10.50	22.0	23.6	7.88E-09	7.60E-08	2:11 PM: TUBING SHIFT
2491	L73-17	10.52	22.0	23.9	2.32E-08	8.30E-08	
2701	L73-18	10.51	22.0	23.7	6.03E-08	6.38E-08	
2847	L73-19	10.66	22.0	23.5	-1.33E-10	3.23E-08	
3532	L73-20	10.55	22.0	23.7	3.97E-09	6.66E-08	
3680	L73-21	10.52	22.0	23.6	1.32E-07	8.39E-08	
3868	L73-22	10.58	22.0	23.7	-1.33E-10	1.12E-07	
4002	L73-23	10.73	22.0	23.7	7.55E-08	1.63E-07	

L74: 23.5°C, P_{O2} = 0.10 atm, pH = 8.2

Time passed (minutes)	Label	Dilution factor (by mass)	T (bath)	T (vessel)	Cu (Molar)	Fe (Molar)	Notes
0	L74-0	10.82	N/A	N/A	0.00E+00	0.00E+00	blank during purge
2	L74-1	10.63	22.0	~20	-1.71E-08	-2.76E-08	fill @ 3:34:26 PM, GAS @ 3:32 (vessel purged)
5	L74-2	10.68	22.0	20.0	-1.71E-08	-3.19E-08	
11	L74-3	10.62	22.0	20.6	-1.71E-08	-1.07E-08	
16	L74-4	10.63	22.0	21.1	-1.71E-08	2.80E-08	
51	L74-6	10.53	22.0	23.0	-1.71E-08	-3.87E-08	
129	L74-7	10.31	22.0	23.2	-1.71E-08	-8.57E-08	
391	L74-8	10.39	22.0	23.5	-1.71E-08	-1.09E-07	
945	L74-9	10.29	22.0	23.5	-1.71E-08	-1.49E-07	
1182	L74-10	10.56	22.0	24.0	-1.71E-08	-9.92E-08	
1414	L74-11	10.39	22.0	24.0	-1.71E-08	-6.02E-08	
1635	L74-12	10.51	22.0	23.5	-1.71E-08	-6.23E-08	NO PRECIP SEEN (L73 has visible precip in tubes)...slower bubbles than L73?
2475	L74-14	10.29	22.0	23.0	-1.71E-08	-5.07E-08	
2613	L74-15	10.23	22.0	23.5	-1.71E-08	-6.48E-08	
2823	L74-16	10.45	22.0	24.0	-1.71E-08	-1.19E-07	2:11 PM: TUBING SHIFT
3024	L74-17	10.33	22.0	24.0	-1.71E-08	-1.01E-07	
3169	L74-18	10.44	22.0	23.5	-1.71E-08	-9.74E-08	
4184	L74-21	10.63	22.0	23.9	-1.71E-08	-1.21E-07	During break down of experiments: WHITE PRECIP SEEN IN TUBES. It probably happened before this because mesh contained a large amount of precip.

L75: 22.0°C, P_{O2} = 0.995 atm, pH = 2.2

Time passed (minutes)	Label	Dilution factor (by mass)	T (bath)	T (vessel)	Cu (molar)	Fe (molar)	Notes
0	L75-0	10.64	N/A	N/A	0.00E+00	0.00E+00	blank during purge
2.5	L75-1	10.52	~19	~20	1.59E-08	-1.88E-07	fill @ 1:37:12 PM, O2 @ 1:38:51 PM
5	L75-2	10.37	~19	~20	4.02E-08	2.38E-07	
10	L75-3	10.27	19.5	20.6	4.37E-08	-7.33E-08	
36	L75-4	10.54	19.5	22.0	1.41E-07	2.65E-07	
75	L75-5	10.52	19.5	22.0	5.00E-08	-1.53E-07	
139	L75-6	10.58	19.5	22.0	8.70E-08	3.07E-08	
202	L75-7	10.48	19.7	22.0	1.11E-07	-1.42E-07	
303	L75-8	10.52	19.5	22.0	1.31E-07	-1.57E-07	
410	L75-9	10.62	19.6	21.8	1.87E-07	-7.09E-08	
568	L75-10	10.51	19.6	21.5	2.11E-07	-6.79E-08	
1013	L75-11	10.63	19.6	21.5	3.20E-07	7.62E-10	
1221	L75-12	10.60	19.6	22.0	3.82E-07	5.78E-08	
1453	L75-13	10.59	19.9	22.0	3.98E-07	1.36E-07	
1650	L75-14	10.72	19.9	22.0	3.90E-07	1.41E-07	
1813	L75-15	10.56	20.0	22.0	5.11E-07	1.74E-07	
2020	L75-16	10.63	19.7	21.8	4.61E-07	3.21E-07	
2637	L75-17	10.54	19.9	22.0	4.92E-07	1.43E-07	
2809	L75-18	9.71	19.6	22.0			
3010	L75-19	10.51	19.6	22.0	5.30E-07	2.63E-07	
3233	L75-20	10.54	19.5	21.8	5.86E-07	2.17E-07	TUBING SHIFT: 3:29 PM
3459	L75-21	10.56	19.5	21.3	6.42E-07	3.08E-07	
4097	L75-22	10.62	19.6	21.9	6.23E-07	2.19E-07	
4222	L75-23	10.56	19.6	22.0	6.32E-07	2.93E-07	
4419	L75-24	10.78	19.6	22.0	6.61E-07	2.58E-07	

L76: 22.0°C, P_{O2} = 0.995 atm, pH = 2.2

Time passed (minutes)	Label	Dilution factor (by mass)	T (bath)	T (vessel)	Cu (molar)	Fe (molar)	Notes
0	L76-0	10.52	N/A	N/A	0.00E+00	0.00E+00	blank during purge
4.5	L76-1	10.40	19.5	20.2	-4.31E-08	1.04E-07	fill @ 2:42:55 PM, O2 @ ~2:45:20 PM, HAD TO SWITCH PUMP HEAD BEFORE FILL!!
6	L76-2	10.36	19.5	20.4	-2.82E-08	2.30E-07	
9	L76-3	10.43	19.5	20.9	-6.26E-09	1.68E-07	
24	L76-4	10.46	19.5	21.4	6.92E-08	5.62E-07	
56	L76-5	10.59	19.5	22.1	-1.10E-08	2.78E-07	
118	L76-6	10.41	19.7	22.2	4.10E-09	2.37E-07	
221	L76-7	10.63	19.5	22.2	7.40E-08	3.36E-07	
328	L76-8	10.23	19.6	22.0	7.61E-08	3.02E-07	
486	L76-9	10.38	19.6	21.8	8.52E-08	3.39E-07	
941	L76-10	10.49	19.6	21.8	2.44E-07	5.43E-07	
1149	L76-11	10.49	19.6	22.0	3.26E-07	5.16E-07	
1381	L76-12	10.57	19.9	22.2	3.49E-07	5.95E-07	
1578	L76-13	10.60	19.9	22.2	3.93E-07	6.51E-07	
1741	L76-14	10.52	20.0	22.2	4.43E-07	7.75E-07	
1949	L76-15	10.42	19.7	21.9	5.67E-07	7.61E-07	BUBBLES UP just BEFORE sample
2564	L76-16	10.39	19.9	22.0	6.62E-07	9.27E-07	
2736	L76-17	10.57	19.6	22.1	7.07E-07	9.88E-07	
2938	L76-18	10.47	19.6	22.1	7.87E-07	9.76E-07	
3161	L76-19	10.35	19.5	22.1	7.36E-07	1.05E-06	TUBING SHIFT: 3:29PM
3386	L76-20	10.54	19.5	21.9	9.06E-07	1.15E-06	
4025	L76-21	10.38	19.6	22.1	8.86E-07	1.05E-06	
4150	L76-22	10.51	19.6	22.2	9.43E-07	1.12E-06	
4347	L76-23	10.68	19.6	22.3	1.03E-06	1.23E-06	

L77: 23.0°C, P_{O_2} = 0.995 atm, pH = 2.7

Time passed (minutes)	Dilution factor (by mass)	T (bath)	T (vessel)	Cu (molar)	Fe (molar)	Notes
0	10.54	N/A	N/A	0.00E+00	0.00E+00	blank AFTER fill (from separatory flask)
2.5	10.47	~18	~20	3.10E-08	1.43E-07	fill @ 3:31:45PM, O2 @ 3:33:43
10	10.41	~21	19.9	3.78E-08	2.65E-07	BATH ON
20	10.58	21.5	20.5	1.10E-07	1.40E-07	3:43: O2 SPLIT for L78
41	10.42	22.0	21.0	2.42E-08	1.70E-07	VESSEL TIPPED OVER (no antifreeze in or spillage, everything remained sealed)
64	10.48	22.0	22.3	1.85E-08	1.35E-07	
116	10.49	22.0	23.0	4.73E-08	2.78E-07	
171	10.39	22.0	23.0	9.39E-08	4.04E-07	
218	10.24	22.0	23.0	4.44E-08	1.17E-07	
375	10.36	22.0	23.0	5.86E-08	3.66E-07	
821	10.26	22.0	22.7	1.25E-07	3.35E-07	
1029	10.44	22.0	23.0	1.57E-07	4.39E-07	
1260	10.46	22.0	23.0	2.77E-07	5.49E-07	2 PM: bubbles DOWN
1620	10.41	22.0	23.0	2.94E-07	4.67E-07	
1828	10.35	22.0	22.6	2.99E-07	4.57E-07	
2445	9.85	22.0	23.0	4.12E-07	5.87E-07	
2556	10.35	22.0	23.0	4.40E-07	8.66E-07	
2759	10.54	22.0	23.0	4.68E-07	5.49E-07	3:32 PM: TUBING SHIFT
3146	10.44	22.0	22.5	5.21E-07	7.27E-07	
3785	10.38	22.0	23.0	6.02E-07	6.84E-07	
3910	10.52	22.0	23.0	6.31E-07	7.46E-07	
4089	10.49	22.0	23.0	5.81E-07	6.46E-07	
4190	10.58	22.0	23.0	6.33E-07	6.96E-07	

L78: 23.5°C, P_{O2} = 0.995 atm, pH = 3.0

Time passed (minutes)	Label	Dilution factor (by mass)	T (bath)	T (vessel)	Cu (molar)	Fe (molar)	Notes
0	L78-0	10.55	N/A	N/A	0.00E+00	0.00E+00	blank AFTER fill
3	L78-1	10.34	22.0	~20	2.90E-08	8.21E-08	fill @ 4:30:48 PM, O2 @ 3:33:06
7	L78-2	10.45	22.0	20.7	6.87E-09	4.25E-08	
13	L78-3	10.51	22.0	21.1	3.05E-09	3.30E-08	
35	L78-4	10.42	22.0	22.3	3.29E-08	5.76E-08	
59	L78-5	10.54	22.0	23.1	3.19E-08	2.07E-07	
93	L78-6	10.54	22.0	23.8	7.19E-08	1.79E-07	
112	L78-7	10.50	22.0	23.9	3.84E-08	2.28E-07	
219	L78-8	10.20	22.0	23.9	5.19E-08	1.83E-07	
372	L78-9	10.29	22.0	23.5	8.56E-08	1.72E-07	
822	L78-10	10.45	22.0	23.4	1.62E-07	3.56E-07	
1262	L78-12	10.53	22.0	24.0	2.13E-07	4.37E-07	
1460	L78-13	10.48	22.0	23.8	2.93E-07	5.57E-07	2 PM: bubbles DOWN
1622	L78-14	10.42	22.0	23.9	2.51E-07	6.74E-07	
1830	L78-15	10.36	22.0	23.4	2.44E-07	4.62E-07	
2450	L78-16	10.10	22.0	23.5	2.92E-07	4.70E-07	
2557	L78-17	10.40	22.0	23.9	3.33E-07	5.99E-07	
2761	L78-18	10.39	22.0	23.9	3.27E-07	5.40E-07	
2982	L78-19	10.30	22.0	23.9	3.55E-07	6.21E-07	TUBING SHIFT @ 3:32 PM
3208	L78-20	10.71	22.0	23.5	3.82E-07	6.71E-07	
3847	L78-21	10.13	22.0	23.7	4.27E-07	5.48E-07	
3971	L78-22	10.41	22.0	24.0	4.12E-07	5.97E-07	
4151	L78-23	10.52	22.0	23.9	4.49E-07	8.83E-07	
4252	L78-24	10.55	22.0	23.9	4.37E-07	6.70E-07	

Appendix D: Data plots for all runs incorporated into the rate law

L52: pH 3.0, P_{O_2} = 0.995 atm, 9.0^{O}C

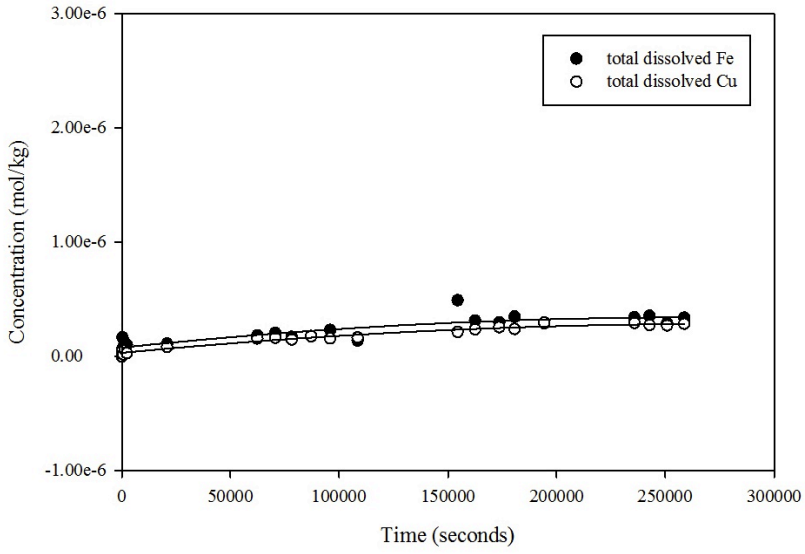

L55: pH 3.0, P_{O_2} = 0.995 atm, 8.5^{O}C

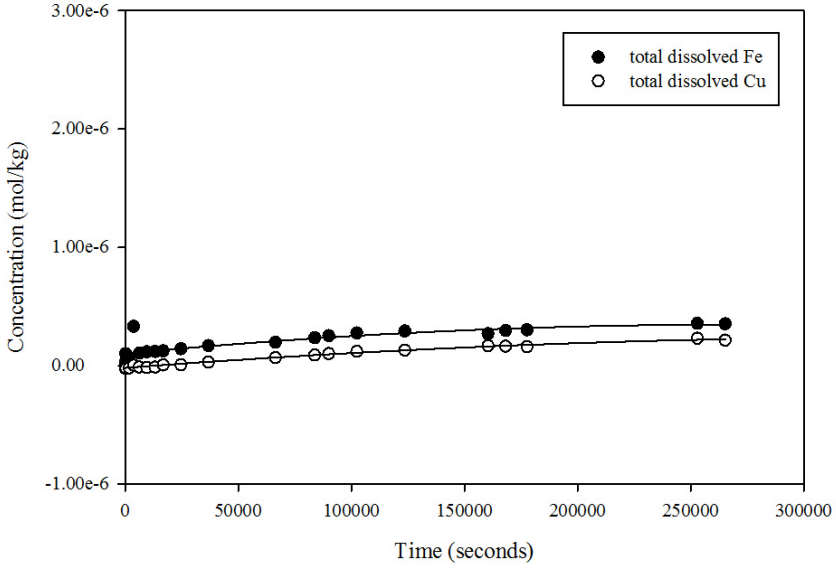

L59: pH 3.1, P_{O_2}= 0.10 atm, 21.0^{O}C

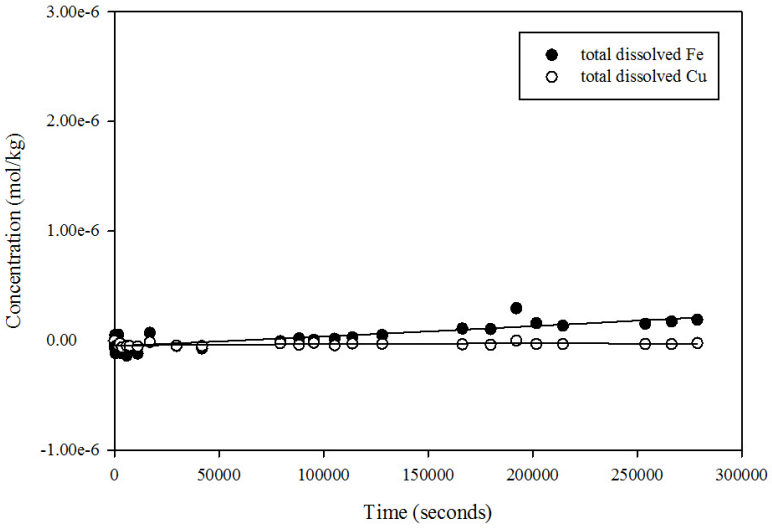

L60: pH 3.0, P_{O_2}= 0.10 atm, 21.0^{O}C

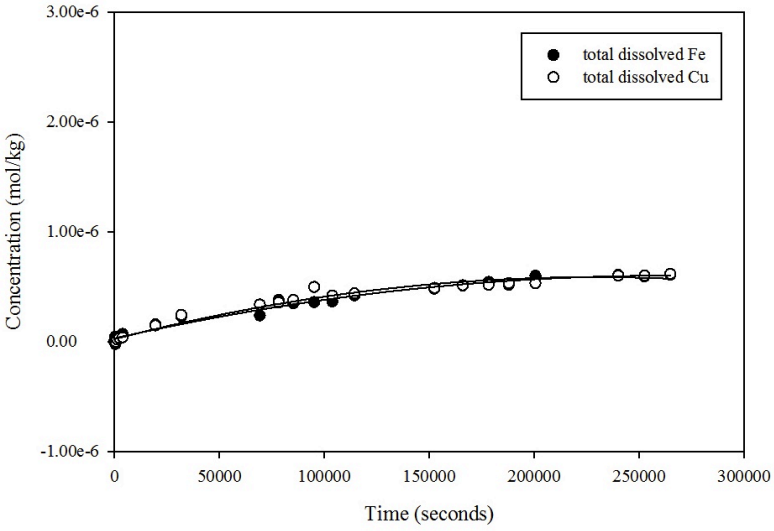

L67: pH 3.2, P_{O_2} = 0.995 atm, 21.5^{O}C

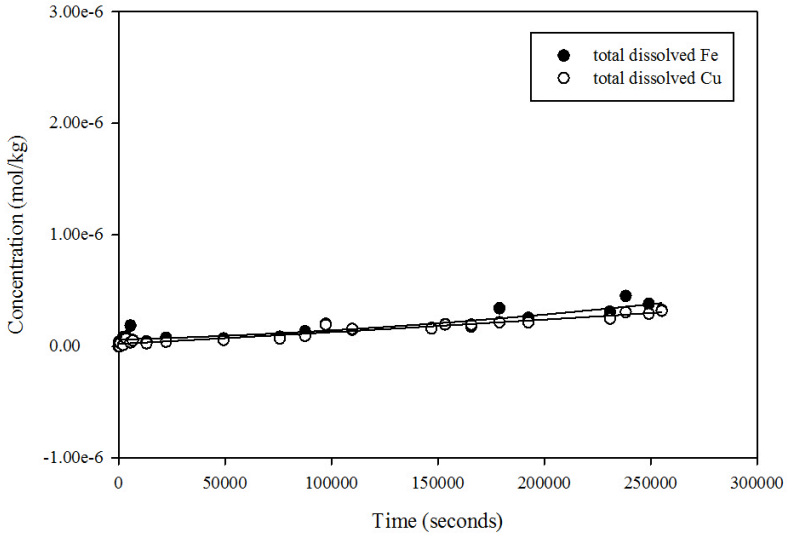

L68: pH 4.5, P_{O_2} = 0.995 atm, 22.0^{O}C

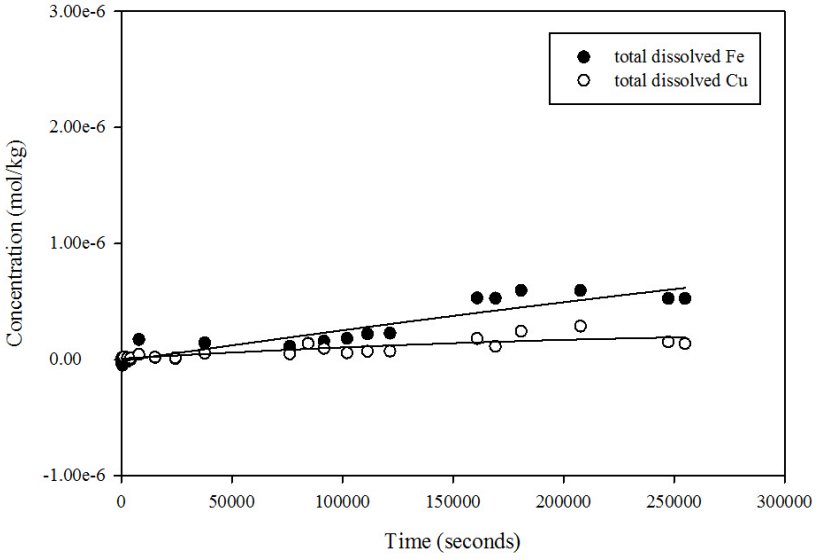

L69: pH 4.0, P_{O_2} = 0.995 atm, 22.5^{O}C

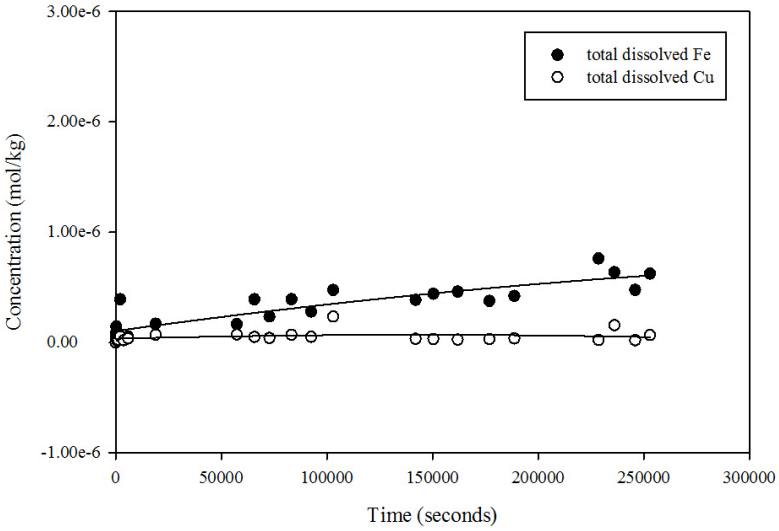

L70: pH 4.1, P_{O_2} = 0.995 atm, 23.0^{O}C

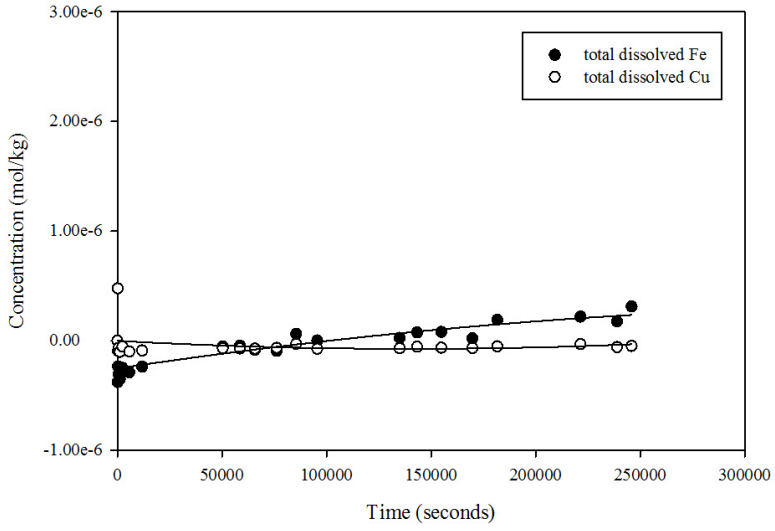

L73: pH 8.2, P_{O_2} = 0.10 atm, 23.5^{O}C

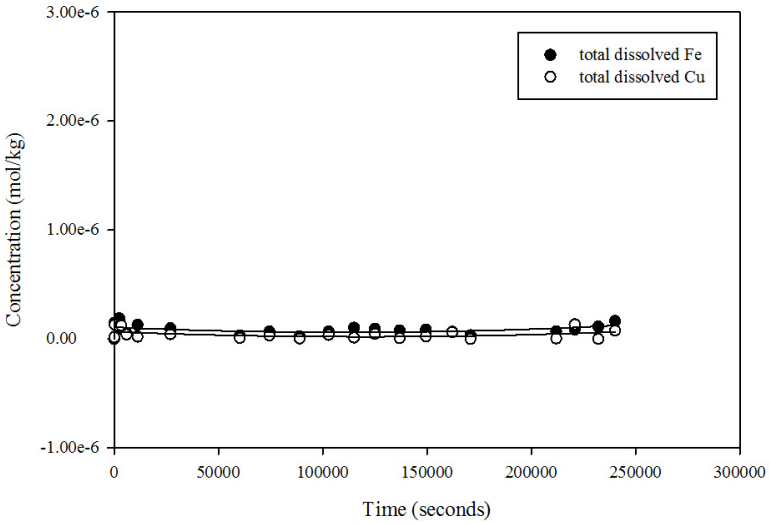

L74: pH 8.2, P_{O_2} = 0.10 atm, 23.5^{O}C

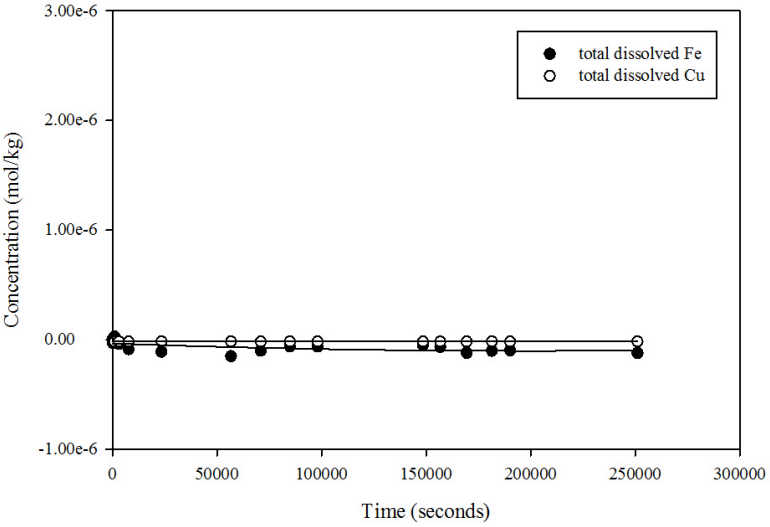

L75: pH 2.2, P_{O_2} = 0.995 atm, 22.0^{O}C

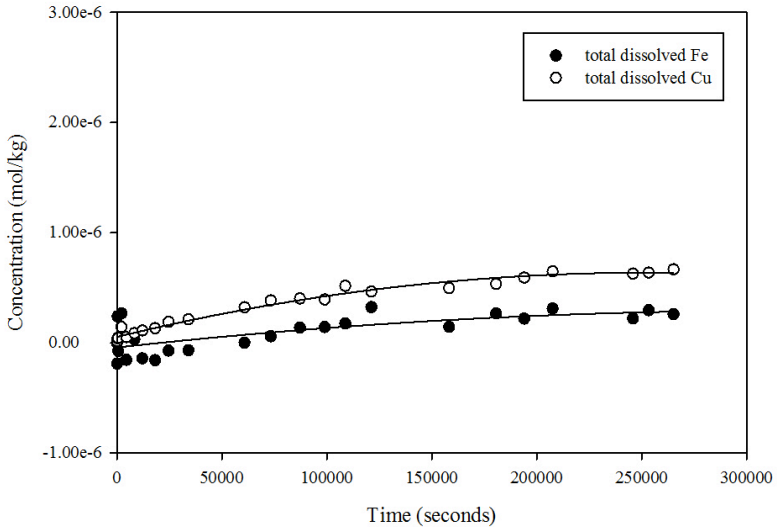

L76: pH 2.2, P_{O_2} = 0.995 atm, 22.0^{O}C

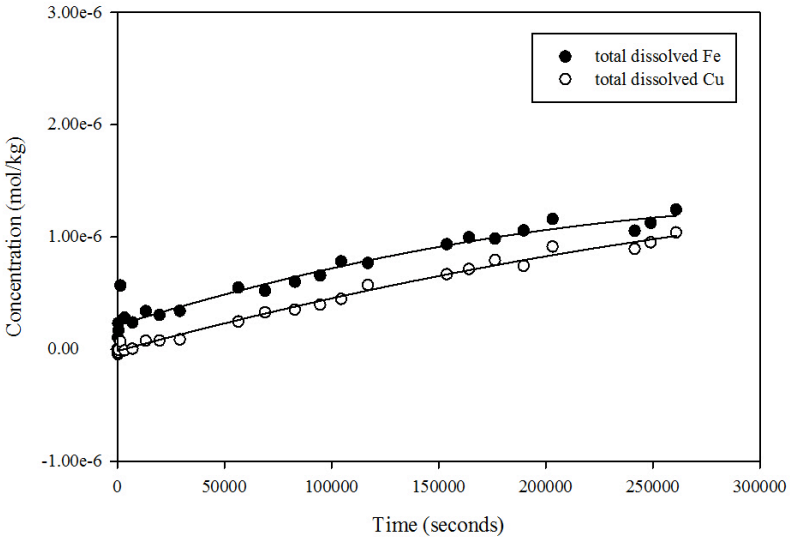

L77: pH 2.7, P_{O_2} = 0.995 atm, 23.0^{O}C

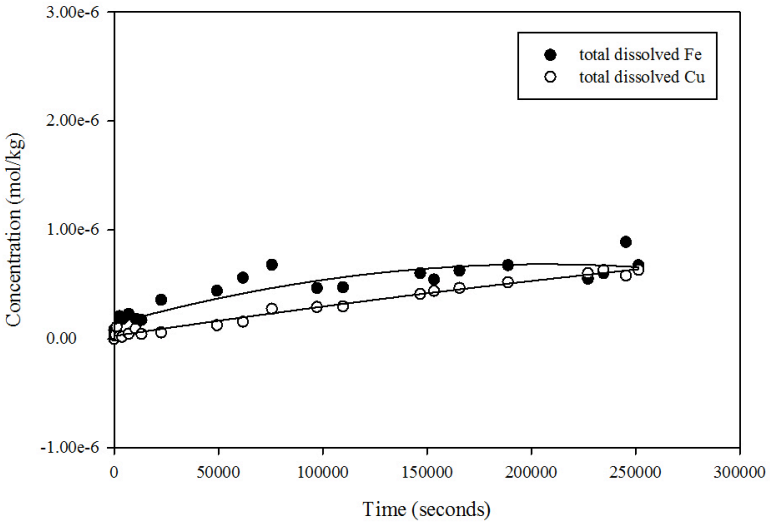

L78: pH 3.0, P_{O_2} = 0.995 atm, 23.5^{O}C